bioRxiv preprint doi: https://doi.org/10.1101/2023.03.18.533278; this version posted March 19, 2023. The copyright holder for this preprint (which was not certified by peer review) is the author/funder, who has granted bioRxiv a license to display the preprint in perpetuity. It is made available under aCC-BY-NC-ND 4.0 International license.

Title: Host genetic variation guides hepacivirus clearance, chronicity, and liver fibrosis in mice

Authors:

Ariane J. Brown[1], John J. Won[1], Raphael Wolfisberg[2], Ulrik Fahnøe[2], Nicholas Catanzaro[1], Ande West[1], Fernando R. Moreira[1], Mariana Nogueira Batista[3], Martin T. Ferris[4], Colton L. Linnertz[4], Sarah R. Leist[1], Cameron Nguyen[1], Gabriela De la Cruz[5], Bentley R. Midkiff[5], Yongjuan Xia[5], Stephanie A. Montgomery[5,6], Eva Billerbeck[7], Jens Bukh[2], Troels K.H. Scheel[2], Charles M. Rice[3], Timothy P. Sheahan[1]

Affiliations

1 Department of Epidemiology, University of North Carolina at Chapel Hill, Chapel Hill, NC 27599, USA.

2 Copenhagen Hepatitis C Program (CO-HEP), Department of Infectious Diseases, Copenhagen University Hospital, Hvidovre and Department of Immunology and Microbiology, University of Copenhagen, Copenhagen, Denmark.

3 Laboratory of Virology and Infectious Disease, The Rockefeller University, New York, NY, USA.

4 Department of Genetics, University of North Carolina at Chapel Hill, Chapel Hill, NC 27599, USA.

5 Lineberger Comprehensive Cancer Center, University of North Carolina School of Medicine, Chapel Hill, NC 27599, USA.

6 Department of Pathology and Laboratory Medicine, University of North Carolina School of Medicine, Chapel Hill, NC 27599, USA.

7 Department of Medicine, Division of Hepatology, Department of Microbiology and Immunology, Albert Einstein College of Medicine, Bronx, NY, USA

Key Words: Animal models, hepatitis c virus, Collaborative Cross, virus-host interactions, viral hepatitis

bioRxiv preprint doi: https://doi.org/10.1101/2023.03.18.533278; this version posted March 19, 2023. The copyright holder for this preprint (which was not certified by peer review) is the author/funder, who has granted bioRxiv a license to display the preprint in perpetuity. It is made available under aCC-BY-NC-ND 4.0 International license.

Abstract

Background & Aims: Human genetic variation is thought to guide the outcome of hepatitis C virus (HCV) infection but model systems within which to dissect these host genetic mechanisms are limited. Norway rat hepacivirus (NrHV), closely related to HCV, causes chronic liver infection in rats but causes acute self-limiting hepatitis in typical strains of laboratory mice, which resolves in two weeks. The Collaborative Cross (CC) is a robust mouse genetics resource comprised of a panel of recombinant inbred strains, which model the complexity of the human genome and provide a system within which to understand diseases driven by complex allelic variation. ***Approach & Results:*** We infected a panel of CC strains with NrHV and identified several that failed to clear virus after 4 weeks. Strains displayed an array of virologic phenotypes ranging from delayed clearance (CC046) to chronicity (CC071, CC080) with viremia for at least 10 months. Body weight loss, hepatocyte infection frequency, viral evolution, T-cell recruitment to the liver, liver inflammation and the capacity to develop liver fibrosis varied among infected CC strains. ***Conclusions:*** These models recapitulate many aspects of HCV infection in humans and demonstrate that host genetic variation affects a multitude of virus and host phenotypes. These models can be used to better understand the molecular mechanisms that drive hepacivirus clearance and chronicity, the virus and host interactions that promote chronic disease manifestations like liver fibrosis, therapeutic and vaccine performance, and how these factors are affected by host genetic variation.

Introduction

Hepatitis C virus (HCV) causes chronic infection of the liver in a majority of those infected. If untreated, chronic HCV infection can lead to the development of end-stage liver disease including hepatocellular carcinoma (HCC) and cirrhosis and may require liver transplant[1-4]. Curative treatments, although costly, are available yet undiagnosed cases, access to treatment, reinfection, drug resistance development and a lack of an effective vaccine have complicated efforts for global elimination of HCV as a public health threat[2,5]. In addition, it is not yet clear if cure will prevent the subsequent development of HCC[1,2,4]. While human genetic variation (e.g. *IL28B* locus) is thought to guide both the kinetics of spontaneous clearance and chronic infection, animal model systems within which to dissect these host genetic mechanisms are not available[6]. Thus, our understanding of how host genetic variation affects HCV pathogenesis, the

bioRxiv preprint doi: https://doi.org/10.1101/2023.03.18.533278; this version posted March 19, 2023. The copyright holder for this preprint (which was not certified by peer review) is the author/funder, who has granted bioRxiv a license to display the preprint in perpetuity. It is made available under aCC-BY-NC-ND 4.0 International license.

development of chronicity, immunity and vaccine efficacy is hampered by the lack of robust immune competent small animal models.

HCV-related hepaciviruses have been discovered in multiple animal species including horses, non-human primates, wild rodents and bats[7]. In 2014, Norway rat hepacivirus (NrHV) was discovered in rats in New York City to cause chronic liver infection[8]. Many basic aspects of NrHV biology are shared with HCV, including hepatotropism, genome organization, dependence on a liver-specific micro RNA (miR-122) for replication and the use of scavenger receptor B-1 for entry[9-11]. In common lab strains of mice, NrHV causes subclinical self-limiting hepatotropic infection that is cleared in 14-21 days but chronic infection can be initiated via transient depletion of CD4 T-cells prior to infection[9]. Models of chronic hepacivirus infection in fully immune competent mice without immune manipulation are not yet available.

The Collaborative Cross (CC) is a robust mouse genetics resource created by the systematic breeding of eight founder strains encompassing classic inbred, disease model and wild-derived models resulting in the generation of a panel of recombinant inbred (RI) strains, which together model the complexity of the human genome and provide a system within which to understand disease driven by complex allelic variation[12]. The CC contains greater than 90% of the common genetic variation in mouse resources through the presence of uniformly distributed SNPs (>40 million) and indels (>4 million) across the various genomes[13,14]. When applied to virology, the CC has been a powerful tool to both identify better models of human disease, as shown with Ebola virus[15], severe acute respiratory syndrome associated coronavirus (SARS-CoV)[16], West Nile virus[17,18], SARS-

bioRxiv preprint doi: https://doi.org/10.1101/2023.03.18.533278; this version posted March 19, 2023. The copyright holder for this preprint (which was not certified by peer review) is the author/funder, who has granted bioRxiv a license to display the preprint in perpetuity. It is made available under aCC-BY-NC-ND 4.0 International license.

CoV-2[19], and influenza A virus[20], and also to map the genetic determinants responsible for complex phenotypic traits[13].

Here, we describe multiple CC mouse models of chronic hepacivirus pathogenesis. We show that host genetic variation affects hepacivirus chronicity, the host response to infection, hepatocyte infection frequency, liver inflammation, liver fibrosis and viral evolution thus recapitulating many aspects of HCV disease biology. This system can be used to better understand the host genes and molecular mechanisms that guide hepacivirus pathogenesis, liver fibrosis, therapeutic and vaccine performance.

Results

Host genetics is a determinant of acute hepacivirus clearance. Given the profound impact human genetic variation can have on HCV infection, we aimed to determine if host genetic variation would affect NrHV pathogenesis and infection kinetics in mice (Fig. 1A). We infected ten different CC mouse strains with a mixture of two sub-populations of mouse derived NrHV inoculum, NrHV-A and -B along with a putative mouse adapted NrHV-B[9] (B_{SLIS}) at a ratio of 1:1:1 (A:B:B_{SLIS}) (Fig. S1). We utilized this mixture to give the best possible foundation for persistency not knowing which genotype would be optimal in the CC. After infection, we monitored viremia for 4 weeks which is 1-2 weeks after WT C57BL/6J (WT) mice typically clear. All strains of mice became infected following NrHV inoculation (Fig. S2), but most CC strains and WT had cleared the infection by week 4. In contrast, CC040, CC046, CC071 and CC080 remained viremic at week 4 (Fig. 1B) and both CC071 ($P = 0.02$) and CC080 ($P = 0.002$) had significancy elevated levels of viremia. Concurrently, CC071 ($P = <0.0001$) and CC080

bioRxiv preprint doi: https://doi.org/10.1101/2023.03.18.533278; this version posted March 19, 2023. The copyright holder for this preprint (which was not certified by peer review) is the author/funder, who has granted bioRxiv a license to display the preprint in perpetuity. It is made available under aCC-BY-NC-ND 4.0 International license.

(P = 0.001) intrahepatic viral RNA was significantly elevated over WT (Fig. 1C). Gene expression of Mx1, a typical interferon stimulated gene (ISG), was elevated in the livers of CC strains that remained viremic, a sign that sustained virus replication continued to instigate the host (Fig. 1D). All together, these data demonstrate that host genetic variation influences acute hepacivirus clearance.

Host genetics is a determinant of hepacivirus chronicity. We then further characterized a subset of CC strains with sustained NrHV replication at 4 weeks. CC046, CC071 and CC080 are genetically distinct with notably different genomic architectures including at loci likely to be important for the antiviral response such as major histocompatibility complex (MHC), T-cell activation, and type I and III interferons (IFN) (Fig. S3). We infected WT, CC046, CC071 and CC080 mouse strains with NrHV as done above and monitored them for 10 months (Fig. 2A). Interestingly, body weight loss was only observed in CC071 infected mice and only during the first week (Fig. S4 and S5). As expected, WT cleared virus within 3 weeks (Fig. 2B). In contrast, CC046 had sustained replication during weeks 1-4 but ultimately all mice cleared virus by week 7 (Fig. 2B). Notably, the majority of CC071 mice became chronically infected with quantifiable viremia until the termination of the study at week 38-39 (Fig. 2B). CC080 mice had a variety of virologic outcomes where some mice cleared virus in middle (4-7 weeks) or late (8-22 weeks) times but only a minority became chronically infected (Fig. 2B). During the first two weeks of infection, the levels of viremia in CC071 (week 1 P = 0.007, week 2 P = 0.001) and CC080 (week 1 P = 0.036, week 2 P = 0.02) were significantly higher than WT and by week 3, viremia in all three CC strains exceeded

bioRxiv preprint doi: https://doi.org/10.1101/2023.03.18.533278; this version posted March 19, 2023. The copyright holder for this preprint (which was not certified by peer review) is the author/funder, who has granted bioRxiv a license to display the preprint in perpetuity. It is made available under aCC-BY-NC-ND 4.0 International license.

that in WT mice (CC046 P = 0.006, CC071 P = 0.007, CC080 P = 0.04) (Fig. 2C). While all CC strains had measurable viremia in week 5, only CC071 (P = 0.01) remained significantly elevated over WT (Fig. 2C).

To assess infectivity in serum, we passively transferred serum from 10-weeks post infection to naïve WT animals and then monitored viremia over time (Fig. S6). As expected, transfer of serum from aviremic mice (WT and CC046) did not transfer infection to recipient animals (Fig. S6B, S6C) but transfer of serum from viremic CC071 (Fig. S6D) and CC080 (Fig. S6E) mice resulted in infection in recipient animals. Thus, viral RNA associated with significant viremia is infectious. Interestingly, when examining viremia per animal, chronically infected animals experienced periods of relatively consistent levels of viremia followed by drastic increases or decreases suggesting an interplay among virus and the host response (Fig. S7). Altogether, by varying host genetics, a spectrum of virologic outcomes were observed following NrHV infection where all WT mice clear early (< 3 weeks), most CC046 mice clear between weeks 4-7, the majority of CC071 became chronically infected, and CC080 displayed phenotypes seen in both CC046 and CC071(Fig. 2D).

Host genetics determines infection frequency and viral dynamics in the liver. To complement our virologic measures in peripheral blood, we next extended our studies to the liver. Labeling viral genomic RNA via *in situ* hybridization (ISH) revealed a variety of phenotypes. First, clearance phenotypes observed in the periphery were similarly observed in WT and CC046 and most CC071 and some CC080 remained viral RNA ISH positive for the duration of the study (Fig. 3A). Second, the amount of viral RNA per

bioRxiv preprint doi: https://doi.org/10.1101/2023.03.18.533278; this version posted March 19, 2023. The copyright holder for this preprint (which was not certified by peer review) is the author/funder, who has granted bioRxiv a license to display the preprint in perpetuity. It is made available under aCC-BY-NC-ND 4.0 International license.

cell varied widely especially at 2dpi where the amount of viral RNA per cell was greatest in CC071 (Fig. 3A). Third, the average infection frequency varied greatly among the different strains. On 2dpi, the infection frequency for CC046 was 22%, more than 10-fold greater than other strains (Fig. 3B). By 7dpi, the infection frequency in CC071 mice had increased similar levels, still significantly greater than both WT and CC080 mice. By 28dpi, the infection frequency in CC071 mice had increased even further (average frequency = 38.1%) but decreased to levels seen at earlier times by the end of the study (Fig. 3B). In paired tissue samples, we quantitated viral RNA via qRT-PCR. As seen with ISH, CC046 had significantly elevated levels of NrHV RNA at 2dpi (P = 0.03-0.04) compared to other CC strains (Fig. 3C). Like the viremia and ISH data, CC071 had elevated levels of intrahepatic viral RNA over WT and CC046 at both 28dpi and 272dpi. Altogether, the intrahepatic virologic data was concordant with that observed in the periphery but also revealed new insights into the impact of host genetic variation on infection frequency and replication dynamics.

Immune dysregulation is associated with chronic hepacivirus infection. Given the disparate outcomes we had observed thus far, we next aimed to determine if host genetics differentially affected immune responses. First, we performed completed blood count on longitudinal peripheral blood samples from the studies described above. The numbers of total lymphocytes were largely unaffected over time comparing infected and strain matched mock mice (Fig. S8A and B). In contrast, neutrophils were significantly and consistently elevated in NrHV infected CC071 compared to strain matched mock mice in weeks 1 and 2 (Fig. S8C and D). To better understand intrahepatic responses,

bioRxiv preprint doi: https://doi.org/10.1101/2023.03.18.533278; this version posted March 19, 2023. The copyright holder for this preprint (which was not certified by peer review) is the author/funder, who has granted bioRxiv a license to display the preprint in perpetuity. It is made available under aCC-BY-NC-ND 4.0 International license.

we labeled liver tissue sections for CD4 positive cells since CD4 T-cells were previously shown to be important for clearance in WT mice[9]. On 2dpi, clusters of CD4+ cells were observed in the parenchyma and on portal tracts in WT mice, who most rapidly clear virus, whereas the labeling pattern remained unchanged from mock for all infected CC strains (Fig. 4). By 7dpi, periportal CD4+ cells were prominent in WT, CC046 and CC071 mice yet the staining pattern for CC080 remained similar to that in uninfected. By 28dpi, clusters of CD4+ cells in periportal and parenchymal space were readily apparent in all infected CC strains, yet the pattern in WT mice, who had all cleared virus by this time, were like mock. By 39 weeks post infection, WT mice remained unremarkable, but clusters of CD4+ cells around portal tracts remained in all chronically infected CC strains and even in CC046 that had cleared after week 7.

Dysregulation of the transcriptome in strains susceptible to prolonged infection. To determine if early defects in the host response were associated with chronic infection, we analyzed the transcriptional responses (Fig. 5) in the liver of WT and CC mouse strains on 7dpi when significant virologic and immunologic differences were observed. Importantly, via principal component analysis (PCA), we confirmed the global responses among mock and infected groups differed and like samples tended to cluster together (Fig. 5A). The numbers of significantly regulated genes varied with host genetics with CC071 regulating more genes than all other strains (Fig. 5B). Pathway analysis of significantly regulated genes (<1.5 Log fold change over mock, P = 0.05) revealed the differential regulation of canonical pathways associated with innate and adaptive immunity among WT and CC strains (Fig. 5C). In Figure 5D, we show the

bioRxiv preprint doi: https://doi.org/10.1101/2023.03.18.533278; this version posted March 19, 2023. The copyright holder for this preprint (which was not certified by peer review) is the author/funder, who has granted bioRxiv a license to display the preprint in perpetuity. It is made available under aCC-BY-NC-ND 4.0 International license.

209 expression fold change data for select canonical pathways including Pathogen Induced
210 Cytokine Storm Signaling, LXR/IL-1 Mediated Inhibition of RXR Function, Th1 Signaling
211 and LXR/RXR Activation. For all affected pathways shown, the gene expression
212 patterns for CC071 are quite different than those in WT and even those of other CC
213 strains with a noted lack of expression in innate immune (e.g. Tlr1, 6, 7, and 13),
214 chemokine (e.g. Ccl6, Cxcl1, Cxcl10), adaptive immune (e.g. *Cd247*, *Cd3*) and Il-
215 1/inflammasome (e.g. Il1b, Il1rn, IL18rap, NLRP3, etc.) related genes. Coupled with the
216 CD4+ cell labeling data above, collectively these data show that CC strains with
217 prolonged and chronic infection are dysregulated in key innate and adaptive immune
218 pathways as compared to WT mice which most rapidly clear virus.
219
220 **Viral evolution is driven by host genetics.** To determine if viral evolutionary patterns
221 varied with host genetics, we deep sequenced the complete viral open reading frame
222 (ORF) in longitudinal serum samples from select mice that either cleared virus or
223 developed chronic infection (Fig. S9). Virus populations from chronically infected
224 animals (CC071 #41, 43, 46; CC080 #58, 63) evolved over time, as evidenced by the
225 continued animal specific branching and increase in branch length in the dendrogram
226 (Fig. S10A). In contrast, virus populations from CC046 who cleared virus the earliest
227 among CC strains evolved the least (Fig. S10A). Proteins/regions of the genome under
228 positive selection accumulate non-synonymous changes at increased frequency
229 compared to synonymous changes. Thus, we then compared the non-synonymous and
230 synonymous changes (dN/dS) per viral ORF. Regardless of host genetic background

bioRxiv preprint doi: https://doi.org/10.1101/2023.03.18.533278; this version posted March 19, 2023. The copyright holder for this preprint (which was not certified by peer review) is the author/funder, who has granted bioRxiv a license to display the preprint in perpetuity. It is made available under aCC-BY-NC-ND 4.0 International license.

and unlike other portions of the genome, the dN/dS ratio for structural proteins E1 and E2, as well as p7 was increased at all times suggestive of positive selection (Fig. S10B).

We next analyzed the mutational patterns per mouse (Fig. 6). CC071 infected mice (Fig 6A), had more nonsynonymous changes compared to viruses from CC080 (Fig. 6B) or CC046 (Fig. 6C) animals no matter infection outcome. In all three CC mouse strains, the mouse adapted NrHV-B_{SLIS} variant was rapidly selected for likely due to its mutations T190S, V353L, F369I and N550S, which appear to adapt the virus to WT mice[9]. In general, viruses from mice that resolved infection had the fewest additional substitutions but several mutations residing in an MHC-I epitope conserved among mice and rats (T184A, S191F, V196A) were observed in viruses from all strains[21]. In addition, either A698V or C715S appeared to be selected in p7 but rarely together. Interestingly, N550S, predicted to disrupt a glycosylation site, reverted in two of three chronically infected CC071 mice concomitantly with the disruption of another predicted glycosylation site at residues 504-506. Substitution of residue 500 (3/3) and 570 (2/3) was also observed in chronically infected CC071 mice. Further, unique changes linked to persistence were observed in CC071 (R984H in NS3) and CC080 (P1446S/L). Thus, viral evolution, clearance and chronicity were closely linked to host genetics.

The pathologic hallmarks of chronic liver infection vary with time and host genetics. To determine the pathological consequences of acute and chronic NrHV infection, we evaluated hematoxylin and eosin-stained liver tissue sections. The hepatic architecture did not vary among mock infected WT, CC046, CC071 and CC080 mice

bioRxiv preprint doi: https://doi.org/10.1101/2023.03.18.533278; this version posted March 19, 2023. The copyright holder for this preprint (which was not certified by peer review) is the author/funder, who has granted bioRxiv a license to display the preprint in perpetuity. It is made available under aCC-BY-NC-ND 4.0 International license.

(Fig. 7). For WT mice, the kinetics of liver pathology largely mirrored that of virus replication. On 2dpi, randomly distributed foci of inflammatory cells associated with single cell necrosis of hepatocytes were noted but by 7dpi, inflammation was notably increased with moderate lymphocytic inflammation predominantly focused on portal triads along with focal, random small clusters of inflammatory cells in the parenchyma all of which was largely resolved by 28dpi (Fig. 7 and S11). In infected CC046, a mild lymphocytic periportal inflammation was noted 7dpi, which became moderate by 28dpi and persisted although more mildly to the end of the study, 8 months after mice had cleared virus (Fig. 7 and S12). Although liver tissue sections from CC071 mice were unremarkable on 2dpi, by 7dpi, moderate periportal inflammation was observed in infected CC071 mice with increased lymphocytes in circulation (Fig. 7 and S13). By 28dpi, periportal and intraparenchymal inflammation was noted and hepatic nuclear inclusions (Fig. S13 Inset), known to be associated with liver disease such as hepatocellular carcinoma and non-alcoholic fatty liver disease, were observed [22,23]. In addition, karyomegaly (i.e. enlargement of nuclei), known to be associated with abnormal liver function, was observed in CC071 infected mice at 28dpi (Fig. S13)[24]. Unlike WT and CC046, by the end of study, moderate periportal inflammation remained in infected CC071 mice. Like CC071, at 2dpi, liver sections from CC080 infected mice were unremarkable (Fig. 7 and S14). Over time, periportal inflammation and foci of intraparenchymal inflammation increased in frequency and severity which by the end of the study was like that in CC071. Lastly, we performed Masson's Trichrome stain on liver tissue sections from the end of the study (i.e. 272 days post infection) to determine if the chronic infection and inflammation was associated with liver fibrosis (Fig. 8).

bioRxiv preprint doi: https://doi.org/10.1101/2023.03.18.533278; this version posted March 19, 2023. The copyright holder for this preprint (which was not certified by peer review) is the author/funder, who has granted bioRxiv a license to display the preprint in perpetuity. It is made available under aCC-BY-NC-ND 4.0 International license.

277 Remarkably, early bridging fibrosis was observed in chronically infected CC071 mice
278 but not in chronically infected CC080 mice suggesting that genetic factors guide multiple
279 disparate pathologic outcomes.
280
281 **Discussion**
282 Here we describe new mouse models of chronic hepacivirus infection that
283 recapitulate multiple aspects of human HCV infection including high titer replication in
284 the liver, persistent infection with virus evolution over time, chronic liver inflammation
285 and liver fibrosis (Fig. S15)[25,26]. For hepacivirus research, the CC provides new models
286 for the mechanistic study of acute and chronic infection, pathogenesis, immunity and
287 vaccination and should provide insights into how host genetics affects acute and chronic
288 infection at an unprecedented resolution.
289 Hepacivirus and hepatocyte interactions guide the trajectory of infection likely
290 involving but not limited to the interplay of viral innate immune antagonists, antiviral
291 innate immune sensors, innate (e.g. Kupffer cells) and adaptive immune cells (e.g. T-
292 cells), cytokines and chemokines, hepatocyte turnover, and host genetic variation (e.g.
293 *IL28B* SNPs)[27-30]. Here, we describe three genetically distinct mouse strains with a
294 multitude of different hepacivirus infection phenotypes and disease trajectories.
295 Interestingly, CC071 mice also have increased susceptibility to classical flaviviruses
296 such as Zika virus (ZIKV), Powassan virus and West Nile virus but not to the bunyavirus
297 Rift Valley fever virus indicating that this strain is particularly sensitive to the
298 *Flaviviridae*[31-33]. JAK/STAT signaling, a key component of the interferon response,
299 appears to function normally in CC071 as interferon treatment of MEFs from CC071 or

bioRxiv preprint doi: https://doi.org/10.1101/2023.03.18.533278; this version posted March 19, 2023. The copyright holder for this preprint (which was not certified by peer review) is the author/funder, who has granted bioRxiv a license to display the preprint in perpetuity. It is made available under aCC-BY-NC-ND 4.0 International license.

WT results in similar levels of STAT1 phosphorylation suggesting that defects in JAK/STAT signaling is not driving increased flavivirus susceptibility[32]. Neither CC046 nor CC071 appear to have a broad immune deficiency as they are not more susceptible to *Salmonella* Typhimurium infection than WT mice (i.e. 129, 129S2/ SvPasCrl)[34].

There is a dearth of small animal models of chronic hepacivirus infection within which to study the virus and host factors that contribute to pathogenesis, mechanisms of viral evolution and evasion of adaptive immunity. Sophisticated transgenic mice, human liver chimeric mice and even mice reconstituted with both human liver and immune cells have been employed to study HCV infection, but species incompatibility complicates the modeling of immunity and chronic disease[35]. Here, we provide an orthogonal approach with NrHV[9,10,36]. Although CD4 T-cell depletion prior to NrHV infection of WT mice can facilitate chronic infection[9], using the CC, we provide a complementary approach demonstrating chronic infection and fibrosis in mice is possible without immune manipulation and that host genetic variation affects viral evolution. Viral evolution was greatest in CC071 mice, with the majority of change occurring in E1 and E2, presumably the main targets of the neutralizing antibody response. The MHC and T-cell related loci of WT, CC046, CC071 and CC080 are different suggesting the potential for differential adaptive immune responses. It is likely that acute resolving and chronic infection are complex processes involving infected cell intrinsic factors, and innate and adaptive immunity. Genetic differences in all these elements could in principle determine the differential outcomes observed between strains. Unfortunately, MHC haplotypes in CC strains remain largely unknown unlike common WT strains of mice.

bioRxiv preprint doi: https://doi.org/10.1101/2023.03.18.533278; this version posted March 19, 2023. The copyright holder for this preprint (which was not certified by peer review) is the author/funder, who has granted bioRxiv a license to display the preprint in perpetuity. It is made available under aCC-BY-NC-ND 4.0 International license.

In summary, we provide new small animal models of chronic hepacivirus infection, evidence that host genetic variation can profoundly affect the outcome of infection and a model genetic system within which to map the loci guiding virus clearance and chronicity. These models have the power to provide both basic insights into hepacivirus biology, hepatocyte biology, innate and adaptive immunity, mammalian genetics as well as new immunocompetent systems within which to study hepacivirus therapeutic efficacy and vaccine performance. Thus, these and future studies should be of broad interest to the field of infectious disease biology, hepatology and immunology.

Materials and Methods

Recombinant Virus Production

DNA from consensus clones NrHV-A, NrHV-B and the mouse adapted NrHV-B_{SLIS}, carrying the T190S, V353L, F369I and N550S mutations (clones to be published elsewhere), were linearized using *MluI* and purified using DNAclean and concentrator (Zymo). RNA was transcribed from 1 ug of *MluI*-linearized DNA using T7 RiboMAX Express Large Scale RNA Production System (Promega). Template DNA was degraded using RQ1 DNAse for 30 min at 4˚C and RNA was purified using RNAeasy mini kit (Qiagen). 4-week-old NRG mice were injected intra-hepatically using 10 µg of RNA in a maximum volume of 50 µL of PBS+RNA and one week post injection a terminal bleed was performed, and serum was pooled, titrated by qRT-PCR and stored in -80˚C freezer. These passage zero virus stocks were amplified through intravenous infection of new 4-week-old NRG mice (N = 10/virus strain to be amplified) with 10^4 genomic equivalents (GE) after which serum harboring the new passage #1 stocks were

bioRxiv preprint doi: https://doi.org/10.1101/2023.03.18.533278; this version posted March 19, 2023. The copyright holder for this preprint (which was not certified by peer review) is the author/funder, who has granted bioRxiv a license to display the preprint in perpetuity. It is made available under aCC-BY-NC-ND 4.0 International license.

346 harvested, titrated and stored as above. All experiments were performed using passage
347 #1 of each strain mixed in equal amounts (1:1:1).
348
349 **Mouse Infection Studies**
350 All Collaborative Cross (CC) mice were obtained in 2015-2021 from the Systems
351 Genetics Core Facility at the University of North Carolina at Chapel Hill[37]. For the initial
352 CC-strain screen, 9–12-week-old female CC004/TauUnc, CC017/Unc, CC021/Unc,
353 CC024/GeniUnc, CC040/TauUnc, CC044/Unc, CC045/GeniUnc, CC046/Unc,
354 CC071/TauUnc and CC080/TauUnc were obtained N = 8/CC strain. Age and sex
355 matched WT C57BL/6J mice were purchased from Jackson Labs. Mice were
356 anesthetized with a mixture of ketamine/xylazine and then infected via retroorbital
357 injection of 100µl containing $1x10^5$ genome equivalents (G.E.) of recombinant NrHV
358 diluted in DPBS (Gibco) (N = 5/strain). As a negative control, 3 mice/strain
359 were mock infected with DPBS. Mice were weighed daily for the first week of infection
360 and then weekly thereafter. To measure virus replication in live mice, whole blood was
361 collected via submandibular bleed, was allowed to clot at room temperature in snap cap
362 tubes, centrifuged at 9,600 x g for 10 minutes and then serum was transferred to a new
363 tube and stored at -80˚C until analysis. Complete blood count was also performed using
364 a Vetscan HM5c automated veterinary blood analyzer using whole blood collected into
365 EDTA tubes. At the end of week 4, animals were euthanized by isoflurane overdose,
366 whole blood and serum were collected and treated as above. Liver tissue was collected
367 from each animal and stored in RNAlater (Thermo) at -80˚C or in 10% formalin prior to
368 processing for histology.

bioRxiv preprint doi: https://doi.org/10.1101/2023.03.18.533278; this version posted March 19, 2023. The copyright holder for this preprint (which was not certified by peer review) is the author/funder, who has granted bioRxiv a license to display the preprint in perpetuity. It is made available under aCC-BY-NC-ND 4.0 International license.

For the subsequent two follow up studies, 7–14-week-old female CC046/Unc (CC046) (N = 17 NrHV infected, 13 mock infected), CC071/TauUnc (CC071) (N = 28 NrHV infected, 19 mock infected) and CC080/TauUnc (CC080) (N = 15 NrHV infected, 14 mock infected) were purchased from the UNC Systems Genetics Core in January through March 2019. Age and sex matched WT C57BL/6J mice were purchased from Jackson Labs (N = 23 NrHV infected, N = 17 mock infected). Mice were infected and followed for the first six weeks as described above. Bleeds and weights then performed every other week for 8 weeks followed then by monthly assessments. These studies were terminated after 37-38 weeks, and blood and tissue were collected as noted above.

RNA isolation, qRT-PCR and Illumina Deep Sequencing

For reverse transcription – quantitative polymerase chain reaction (qRT-PCR) quantitation of viral RNA in serum, RNA was isolated from 5µl of mouse serum using the RNA Clean & Concentrator -5 (Zymo) or High Pure Viral Nucleic Acid kit (Roche) kits. qRT-PCR was performed using 5µl of eluted RNA, TaqMan Fast Virus 1-step Master Mix (Applied Biosystems) and primer/probes targeting NS3 primers/probe (IDT)[11]. The sequence of the NrHV NS3 primers and probes were: Primer 1: AAGCGCAGCACCAATTCC, Primer 2: TACATGGCTAAGCAATACGG, Probe: /56-FAM/CTCACGTAC/ZEN/ATGACGTACGGCATG/3IABkFQ/. NrHV standard curve RNA (MEGAscript, Thermo) was produced by PCR amplification of NS3 downstream of a T7 promoter. Reactions were performed in LightCycler 480 Multiwell Plates (Roche) in a LightCycler 480 (Roche) using the following program: 50°C for 30 minutes, 95°C for 5

bioRxiv preprint doi: https://doi.org/10.1101/2023.03.18.533278; this version posted March 19, 2023. The copyright holder for this preprint (which was not certified by peer review) is the author/funder, who has granted bioRxiv a license to display the preprint in perpetuity. It is made available under aCC-BY-NC-ND 4.0 International license.

minutes, followed by 40 cycles of 95°C for 15 seconds, 56°C for 30 seconds, and 60°C for 45 seconds, then 40°C for 10 seconds. For qRT-PCR to quantitate NrHV RNA, ISG expression and mRNA sequencing in liver tissue, liver tissue was homogenized in TRIzol reagent (Thermo), and RNA was isolated according to protocol. 500ng total RNA was utilized for each qRT-PCR reaction. ISG MX dynamin-like GTPase 1 (Mx1, Thermo Fisher, Mm00487796_m1) expression was assessed in select samples. Relative expression of Mx1 to housekeeping gene glyceraldehyde-3-phosphate dehydrogenase (GAPDH, Thermo Fisher, Mm99999915_g1) was calculated by ΔΔCT method[38]. Illumina total RNA-seq was performed by the UNC High Throughput Sequencing Facility (HTSF). Stranded mRNA libraries were prepared (Kapa mRNA) and read on the Illumina HiSeq4000 platform (single end 1x50 read length). For analysis of raw reads, sequenced reads were mapped to the mouse reference transcriptome (Ensemble; Mus musculus version 108) using Kallisto (version 0.46.0). Transcript quantification data was normalized using the TMM method in EdgeR (version 3.38.4) and differentially expressed genes (p.Adj.val < 0.05; logLC > 1.5) were identified using linear modeling with limma (version 3.52.2) using R (version 4.2.0) in R Studio (version 2022-04-19). Gene ontology analysis was carried out using the Ingenuity Pathway Analysis (Qiagen). Heat maps were generated using Broad Institute's Morpheus web application (https://software.broadinstitute.org/morpheus/). Hierarchical clustering was performed by One Minus Pearson Correlation with Average Linkage clustering by columns and rows. Sequence data is available on the Gene Expression Omnibus (GEO, accession # GSE###).

bioRxiv preprint doi: https://doi.org/10.1101/2023.03.18.533278; this version posted March 19, 2023. The copyright holder for this preprint (which was not certified by peer review) is the author/funder, who has granted bioRxiv a license to display the preprint in perpetuity. It is made available under aCC-BY-NC-ND 4.0 International license.

Liver Pathology and Digital Quantitation of Viral RNA in Liver Tissue Sections

To assess liver pathology, we formalin fixed, paraffin embedded liver tissues, generated sections (~5µm) and stained then with hematoxylin/eosin (Richard-Allen Scientific) on an Autostainer XL from Leica Biosystems. To assess liver fibrosis, sections were stained using Masson's Trichrome (Richard-Allen Scientific). For CD4 immunohistochemical (IHC) staining, antigen retrieval (20 minutes at 100˚C in Leica Bond-Epitope Retrieval Solution 2 pH-9) was performed on dewaxed tissues prior to labeling with CD4 antibody (ab183685, Abcam) at 1:2,000 for 1h followed with Novolink Polymer (RE7260-CE) secondary antibody labeling on a Leica Bond III Autostainer. Antibody labeling was detected using 3,3'-diaminobenzidine (DAB) and the Bond Intense R detection system (DS9263). Tissue sections were evaluated by a Board Certified Veterinary pathologist.

NrHV viral RNA was visualized in liver tissue sections by *in situ* hybridization (ISH) using RNAscope probes (Item # V-NrHV-PP) designed by Advanced Cell Diagnostics based on the whole genome sequence of NrHV (Genebank Accession # MF113386.1). ISH on liver tissue sections was performed on a Leica Rx autostainer (Leica Biosystems) with a hematoxylin counterstain. For quantitation, slides were scanned on a Versa slide scanner (Leica Biosystems) with a 40X power objective and a Point Gray camera (8-bit image at 0.137152 microns/pixel) and imported to Definiens Architect XD 2.7 for analysis with Tissue Studio version 4.4.2. Per tissue section per animal, total tissue area was calculated and total numbers of cells per section was calculated using the nuclear counterstain as a guide. Similar numbers of cells were assessed in each tissue section per timepoint. NrHV positive cells were identified by

bioRxiv preprint doi: https://doi.org/10.1101/2023.03.18.533278; this version posted March 19, 2023. The copyright holder for this preprint (which was not certified by peer review) is the author/funder, who has granted bioRxiv a license to display the preprint in perpetuity. It is made available under aCC-BY-NC-ND 4.0 International license.

ISH positivity. The spot size threshold was 1.5 μm². Spot areas were ranked as None/Low (2 μm²), Low/Medium (6 μm²), or Medium/High (10 μm²). Resultant data was used to determine the infection frequency per tissue section.

Deep sequencing NrHV genomes

Serum from NrHV infected mice was diluted in PBS (25 μL in 225 μL PBS), added to a 2 mL Phasemaker tube (Thermo Fisher Scientific), mixed with 750 μL TRIzol LS Reagent (Thermo Fisher Scientific) after which 200 μl chloroform was added, shaken for 15 seconds, incubated for 3 min at room temperature, and centrifugated at 12,000g for 15 min at 4°C. The aqueous phase was removed and mixed with 450 μl ethanol and transferred to an RNA Clean & Concentrator-5 column (Zymo Research) for downstream RNA purification and concentration. Reverse-transcription (RT) was performed with Maxima H Minus Reverse Transcriptase (Thermo Fisher Scientific). Samples were pre-incubated in the presence of RNase inhibitors (Promega) at 65°C for 2 min prior to addition of the RT enzyme, followed by incubation at 50°C for 2h using 0.1 μM primer TS-O-00319 (GCTTCCTGGAGCGGGCTAGATACTG). Amplification of the complete ORF was performed using Q5 Hot Start High-Fidelity DNA Polymerase (New England Biolabs), including high GC Enhancer, and the primer pair Reverse TS-O-00318 (CCAAGCCCCAATGCCGTCCGGCACCGCTGCCCTTTTCGG) and Forward TS-O-00361 (AGGTGAAGGGGGCATCGATG) (0.5 μM each). The PCR cycling parameters were 98°C for 30 s, followed by 37 cycles of 98°C for 10 s, 65°C for 10 s and 72°C for 8 min, with a final extension at 72°C for 10 min. Amplified DNA was purified using DNA Clean & Concentrator-25 columns (Zymo Research), and libraries

bioRxiv preprint doi: https://doi.org/10.1101/2023.03.18.533278; this version posted March 19, 2023. The copyright holder for this preprint (which was not certified by peer review) is the author/funder, who has granted bioRxiv a license to display the preprint in perpetuity. It is made available under aCC-BY-NC-ND 4.0 International license.

461 for deep sequencing were prepared using the NEBNext Ultra II FS DNA Library Prep Kit
462 for Illumina (New England Biolabs). Quality of DNA libraries was validated using a 2100
463 Bioanalyzer Instrument (Agilent). DNA libraries were quantitated via Qubit dsDNA High-
464 Sensitivity Assay Kit (Thermo Fisher Scientific) and libraries were pooled in equimolar
465 concentrations prior to denaturation. Pooled libraries were loaded on a MiSeq v3 150
466 cycle flow-cell, and sequencing performed on a MiSeq benchtop sequencer (Illumina).
467 Analysis was performed as previously described[10,39], In short, pair-end reads were
468 trimmed and filtered by Sickle and subsequently mapped by BWA onto the NrHV-B
469 reference (GenBank: ON758386) using the MEM algorithm. Samtools were used to
470 process the alignment files and Lofreq were applied to call SNPs that were translated by
471 SNPEffect. Multiple mutations in the same specific codons were subsequently resolved
472 by LinkGE. Pairwise distance and dN/dS ratios were calculated form the vcf files by
473 SNPGenie.
474
475 **Author Contributions:** TPS, MTF, CMR, JB and TKHS designed the studies. AJB, JW,
476 RW, UF, NC, AW, FRM, MTF, CLL, SRL, CN, GDLC, BRM, YX, SAM, and TPS
477 performed the studies. EB, MNB and CMR provided recombinant NrHV for these
478 studies. TPS, RW, UF, EB, SAM, TKHS, JB and CMR wrote and edited the manuscript.
479 All authors read and approved this manuscript.
480
481 **Acknowledgements:** This work was funded by R01 grant from the National Institute of
482 Allergy and Infectious Disease (NIAID, AI131688 to C.M.R.), a U19 grant from NIAID
483 (U19AI100625 to Ralph Baric and Mark Heise), the Independent Research Fund

bioRxiv preprint doi: https://doi.org/10.1101/2023.03.18.533278; this version posted March 19, 2023. The copyright holder for this preprint (which was not certified by peer review) is the author/funder, who has granted bioRxiv a license to display the preprint in perpetuity. It is made available under aCC-BY-NC-ND 4.0 International license.

Denmark (1030-00426 to Troels K. H. Scheel), Advanced Grant 4004-00598 to Jens Bukh), the Danish Cancer Society (R204-A12639 to Jens Bukh and Troels K. H. Scheel), the Novo Nordisk Foundation (Distinguished Investigator Grant NNF19OC0054518 and Tandem NNF19OC0055462 to Jens Bukh), and the European Research Council (Starting Grant 802899 to Troels K. H. Scheel). Raphael Wolfisberg. was supported by an Early Postdoc Mobility Fellowship (P2BEP3_178527) and a Post-doc Mobility Fellowship (P400PB-183952) from the Swiss National Science Foundation. We gratefully acknowledge the technical support from the UNC High Throughput Sequencing Facility. This facility is supported by the University Cancer Research Fund, Comprehensive Cancer Center Core Support grant (P30-CA016086), and UNC Center for Mental Health and Susceptibility grant (P30-ES010126). We would like to thank Louise B. Christensen (Department of Clinical Microbiology, University of Copenhagen) for laboratory assistance and the Department of Clinical Microbiology, Hvidovre Hospital for access to Illumina miSeq equipment. Collaborative Cross (CC)[37] mice were obtained in 2017-2021 from the Systems Genetics Core Facility at the University of North Carolina at Chapel Hill. We would also like to thank Dr. Amit Kapoor from the University of Ohio and Dr. Brad Rosenberg from Mt. Sinai Medical School for helpful and insightful discussion of this work.

Figure Legends

Figure 1. Host genetics is a determinant of acute hepacivirus clearance. (A) Study design. Ten Collaborative Cross (CC) strains and control C57BL/6J female mice 9-13

bioRxiv preprint doi: https://doi.org/10.1101/2023.03.18.533278; this version posted March 19, 2023. The copyright holder for this preprint (which was not certified by peer review) is the author/funder, who has granted bioRxiv a license to display the preprint in perpetuity. It is made available under aCC-BY-NC-ND 4.0 International license.

weeks in age were infected with $1x10^5$ genome equivalents of recombinant NrHV or negative control PBS via retroorbital injection and bled weekly to monitor viremia. Mouse numbers per strain were: C57BL/6J N = 8, CC004 N = 4, CC017 N = 4, CC021 N = 4, CC024 N = 5, CC040 N = 5, CC044 N = 5, CC045 N = 5, CC046 N = 6. CC071 N = 5, CC080 N = 4. For all strains PBS mock infected N = 3. **(B)** Week 4 viremia as determined by qRT-PCR of viral RNA isolated from serum. The dotted line indicates the limit of quantitation. **(C)** Intrahepatic viral load 4 weeks post infection by qRT-PCR using 500 ng total liver RNA. Numbers of mice per group: C57BL/6J (8 NrHV, 4 Mock), CC040 (4 NrHV, 3 mock), CC046 (6 NrHV, 3 mock), CC071 (5 infected, 3 mock), CC080 (4 infected, 3 mock). **(D)** *Mx1* intrahepatic gene expression 4 weeks by qRT-PCR using 500ng total RNA. Data is expressed as fold change over mock infected by ΔΔCT method. For B and D, asterisks indicate statistical significance as determined by Kruskal-Wallis test. For C, asterisks indicate statistical significance by Two-Way ANOVA with a Dunnett's multiple comparison test.

Figure 2. Host genetics is a determinant of hepacivirus chronicity. (A) Study Design. C57BL/6J, CC046, CC071 and CC080 mice were infected with $1x10^5$ genome equivalents of recombinant NrHV or negative control PBS via retroorbital injection and viremia was monitored weekly or monthly. **(B)** NrHV viremia for weeks 1-39 determined by qRT-PCR of RNA from serum. See Table S2 for the numbers of animals per strain per time. **(C)** NrHV Viremia for weeks 1-5. Levels of viral RNA in serum were measured by qRT-PCR. C57BL/6J Time (N): week 1 (19), week 2 (15), week 3 (15), week 4 (15), week 5 (15). CC046 Time (N): week 1 (13), week 2 (10), week 3 (10), week 4 (10),

bioRxiv preprint doi: https://doi.org/10.1101/2023.03.18.533278; this version posted March 19, 2023. The copyright holder for this preprint (which was not certified by peer review) is the author/funder, who has granted bioRxiv a license to display the preprint in perpetuity. It is made available under aCC-BY-NC-ND 4.0 International license.

week 5 (10). CC071 Time (N): week 1 (22), week 2 (20), week 3 (18), week 4 (19), week 5 (19). CC080 Time (N): week 1 (13), week 2 (10), week 3 (10), week 4 (10), week 5 (10). Asterisks indicate statistically significant differences by Two-Way ANOVA Tukey's multiple comparisons test. **(D)** Proportion of mice per strain that clear virus early (< 3 weeks), middle (week 4-7), late (week 8-22) or do not clear (viremic week 23 to end of study). Only mice that survived to the end of the study were considered for this analysis. For B and C, the dotted line indicates the average limit of quantitation. All data for B-D, was compiled from two independent experiments.

Figure 3. Host genetics determines infection frequency and viral dynamics in the liver. (A) NrHV viral RNA *in-situ* hybridization in liver tissue sections from mock or NrHV infected C57BL/6J, CC046, CC071 or CC080 mice 2, 7, 28 or 272 dpi. Nuclei are stained blue and viral RNA is labeled brown. **(B)** Percent cells NrHV RNA positive via RNAscope *in situ* hybridization quantified using Definiens Architect. C57BL/6J Time (N): Mock (6), 2dpi (4), 7dpi (4), 28dpi (5), 272dpi (7). CC046 Time (N): Mock (7), 2dpi (4), 7dpi (3), 28dpi (6), 272dpi (5). CC071 Time (N): Mock (7), 2dpi (4), 7dpi (2), 28dpi (5), 272dpi (15). CC080 Time (N): Mock (6), 2dpi (4), 7dpi (3), 28dpi (4), 272dpi (8). **(C)** NrHV genome copy number in 500ng total liver RNA by qRT-PCR. C57BL/6J Time (N): Mock (4), 2dpi (4), 7dpi (4), 28dpi (5), 272dpi (7). CC046 Time (N): Mock (4), 2dpi (4), 7dpi (3), 28dpi (6), 272dpi (5). CC071 Time (N): Mock (4), 2dpi (4), 7dpi (2), 28dpi (5), 272dpi (15). CC080 Time (N): Mock (4), 2dpi (4), 7dpi (3), 28dpi (4), 272dpi (8). Asterisks in B and C indicate statistical significance by Two-Way ANOVA Tukey's multiple comparisons test.

bioRxiv preprint doi: https://doi.org/10.1101/2023.03.18.533278; this version posted March 19, 2023. The copyright holder for this preprint (which was not certified by peer review) is the author/funder, who has granted bioRxiv a license to display the preprint in perpetuity. It is made available under aCC-BY-NC-ND 4.0 International license.

Figure 4. CD4 cell recruitment is delayed in CC mouse strains. CD4 cell labeling in liver tissue sections from mock and NrHV infected animals at 2, 7, 28, and 272dpi with CD4 cells (brown) and nuclei (blue). Representative images of mouse strains and timepoints are shown.

Figure 5. Dysregulation of the transcriptome in strains susceptible to chronic infection. Total RNA from mock and NrHV infected liver tissue was deep sequenced by Illumina HiSeq 4000. For all groups, N = 3 except for CC071 NrHV infected N =2. **(A)** Principal component analysis of expression data for mock and infected groups. **(B)** Top 40 Regulated Canonical Pathways by Ingenuity IPA. The significance (-log(p-value) and predicted regulation (Z-score) for each pathway is indicated by the scale bar. **(C)** Expression of significantly regulated genes (>1.5 Log fold change $P < 0.05$) over mock in select Canonical pathways. Heat maps were generated in Morpheus.

Figure 6. Host genetics drives differential viral evolution. Amino acid changes observed in the NrHV ORF for **(A)** CC071 animals that clear (#42, 44, 47) and become chronically infected (#41, 43, 46), **(B)** CC080 animals that clear (#57, 60, 61, 62) and become chronically infected (#58 and 63) and **(C)** CC046 animals that clear (#28, 29, 30). The heat map color intensity indicates mutation frequencies (%). Mouse adaptive mutations present in the inoculum (T190S, V353L, F369I, and N550S) are highlighted in hot pink. Changes shared by more than one CC strain are in bold.

bioRxiv preprint doi: https://doi.org/10.1101/2023.03.18.533278; this version posted March 19, 2023. The copyright holder for this preprint (which was not certified by peer review) is the author/funder, who has granted bioRxiv a license to display the preprint in perpetuity. It is made available under aCC-BY-NC-ND 4.0 International license.

Figure 7. The pathologic hallmarks of chronic liver infection vary with time and host genetics. Liver tissue sections from mock or NrHV infected WT, CC046, CC071 and CC080 mice at 2, 7, 28 and 272 dpi were stained with hematoxylin and eosin. Hallmark features of normal liver architecture including portal vein, bile duct, hepatic artery, central vein and hepatocytes are noted in each mock panel.

Figure 8. Liver fibrosis is associated with chronic liver infection. Liver tissue sections from mock or NrHV infected WT, CC046, CC071 and CC080 mice at 272 dpi were stained with Masson's Trichrome which stains collagen blue. Inflammatory cells and early bridging fibrosis are noted.

Supplemental Figures

Figure S1. Deep sequencing of recombinant virus populations utilized for *in vivo* studies. . Associated with main Figure 1. **(A)** The amino acid sequence differences for NrHV-A (Genbank: MF113386), NrHV-B (Genbank ON758386) and B_{SLIS} (NrHV-B with the additional changes T190S, V353L, F369I and N550S) as compared to the RHV-rn1 reference isolate (Genbank: KX905133) virus strain. **(B)** Deep sequencing of the input virus pool which revealed a stoichiometry of 42% A, 19% B, 39% B_{SLIS}. Three additional mutations (207T, 1221P and 1590G) were noted in all B virus sequences likely acquired during stock generation *in vivo*.

Figure S2. NrHV week 1 viremia for 10-strain Collaborative Cross screen. Associated with main Figure 1. Ten CC strains and control C57BL/6J female mice 9-13

bioRxiv preprint doi: https://doi.org/10.1101/2023.03.18.533278; this version posted March 19, 2023. The copyright holder for this preprint (which was not certified by peer review) is the author/funder, who has granted bioRxiv a license to display the preprint in perpetuity. It is made available under aCC-BY-NC-ND 4.0 International license.

weeks in age were infected with $1x10^5$ G.E. of recombinant NrHV or negative control PBS via retroorbital injection and bled weekly to monitor viremia. Infected mouse numbers per strain were: C57BL/6J N = 8, CC004 N = 4, CC017 N = 4, CC021 N = 4, CC024 N = 5, CC040 N = 5, CC044 N = 5, CC045 N = 5, CC046 N = 6. CC071 N = 5, CC080 N = 4. For all strains PBS mock infected N = 3. Levels of viral RNA in 1µl serum as measured by qRT-PCR is shown.

Figure S3. The genetic architecture of Collaborative Cross strains CC046, CC071, and CC080. Associated with main Figure 2. Figure adapted from Leist et al.[40] **(A)** The CC is a recombinant inbred mouse reference population generated by breeding five classic inbred strains (A/J, C57BL/6, 129, NOD and NZO) with three wild strains (CAST, PWK and WSB). **(B)** The proportion of each founder strain comprising each CC strain of interest. **(C)** The genomic architecture of CC046, CC071 and CC080. The color segments of each chromosome pair correspond to loci donated by founder strains. **(D)** The genotype of CC046, CC071 and CC080 at the MHC locus, genes related to T-cell activation and type I and III interferon. The colors in the grid correspond to the genotype at each region.

Figure S4. Body weight for mock and NrHV infected mice. Associated with main Figure 2. C57BL/6J, CC046, CC071 and CC080 mice were infected with $1x10^5$ G.E. of recombinant NrHV or negative control PBS via retroorbital injection. Body weights were measured daily for the first two weeks and then intermittently for the duration of the

bioRxiv preprint doi: https://doi.org/10.1101/2023.03.18.533278; this version posted March 19, 2023. The copyright holder for this preprint (which was not certified by peer review) is the author/funder, who has granted bioRxiv a license to display the preprint in perpetuity. It is made available under aCC-BY-NC-ND 4.0 International license.

621 study to 272 or 273dpi. The percent starting weight is shown for age and strain matched
622 mock PBS infected and NrHV infected over time.
623
624 **Figure S5. Body weight for mock and NrHV infected mice for days 0-14.** Associated
625 with main Figure 2 and Figure S4. C57BL/6J, CC046, CC071 and CC080 mice were
626 infected with $1x10^5$ G.E. of recombinant NrHV or negative control PBS via retroorbital
627 injection. Daily body weights are shown for the first 14 days of infection. Asterisks
628 indicate statistical significance by two-way ANOVA with a Sidak's multiple comparison
629 test.
630
631 **Figure S6. Passive transfer to demonstrate the presence of infectious virus.**
632 Associated with main Figure 2. **(A)** To demonstrate the presence of infectious virus in
633 NrHV RNA positive sera, 5µl of serum from 12 weeks post infection was diluted in 150µl
634 PBS and 100µl of this mixture was used to inoculate naïve C57BL/6J mice via the
635 retroorbital route. **(B)** Transfer of serum from previously infected aviremic C57BL/6J
636 mice to recipient naïve C57BL/6J mice. **(C)** Transfer of serum from previously infected
637 but aviremic CC046 mice to recipient naïve C57BL/6J mice. **(D)** Transfer of serum from
638 viremic CC071 mice to recipient naïve C57BL/6J mice. **(E)** Transfer of serum from three
639 aviremic mice and one viremic CC080 mouse to three recipient naïve C57BL/6J mice.
640
641 **Figure S7. Kinetics of viremia in individual mice with different viral clearance**
642 **phenotypes.** Associated with main Figure 2. The levels of viral RNA in serum as
643 measured by qRT-PCR are shown for C57BL/6J, CC046, CC071 and CC080. Four

bioRxiv preprint doi: https://doi.org/10.1101/2023.03.18.533278; this version posted March 19, 2023. The copyright holder for this preprint (which was not certified by peer review) is the author/funder, who has granted bioRxiv a license to display the preprint in perpetuity. It is made available under aCC-BY-NC-ND 4.0 International license.

644 clearance phenotypes were noted: Early Clearance (< 3 weeks), Middle Clearance
645 (Week 4-7), Late Clearance (Week 8-22), No Clearance (viremic at the end of study
646 week 38/39).
647
648 **Figure S8. Total blood lymphocytes and neutrophils for all times post infection.**
649 Associated with main Figure 4. Complete blood count was performed using a Vetscan
650 HM5 automated blood analyzer on whole blood isolated from mock and infected mice
651 for the duration of studies described in Fig. 2. **(A)** Blood lymphocytes are shown for the
652 first five weeks of infection or **(B)** for the duration of the study for each mouse strain. **(C)**
653 Complete blood count for neutrophils for the first five weeks of infection or **(D)** for the
654 duration of the study for each mouse strain. Asterisks indicate statistically significant
655 differences by Two-Way ANOVA Tukey's multiple comparisons test.
656
657 **Figure S9. Viremia phenotypes for mice on which viral ORF sequencing was**
658 **performed.** Associated with main Figure 6 and Figure S12. The levels of viral RNA in
659 serum as measured by qRT-PCR are shown for C57BL/6J, CC046, CC071 and CC080.
660
661 **Figure S10. Chronic infection is associated with increased viral evolution. (A)**
662 Associated with main Figure 6 and Figure S9. The genetic relationships of virus
663 populations isolated from NrHV infected CC046 (N = 3), CC071 (N = 6) or CC080 (N =
664 6) over time are shown in a neighbor joining tree created from whole viral ORF
665 sequences from 1, 4, 7, 13, 27 and 38 weeks post infection. Infected animals and
666 phenotypes are described in Figure 2. The viremia phenotypes per mouse are

bioRxiv preprint doi: https://doi.org/10.1101/2023.03.18.533278; this version posted March 19, 2023. The copyright holder for this preprint (which was not certified by peer review) is the author/funder, who has granted bioRxiv a license to display the preprint in perpetuity. It is made available under aCC-BY-NC-ND 4.0 International license.

667 described in Figure S9. The dendrogram was generated by aligning full ORF sequences
668 by MAFFT and building the phylogeny by maximum likelihood using PhyML using the
669 general time reversible substitution model and rooted the inoculum input of the current
670 study and the rat inoculum used for NRG mouse adaptation (NrHV-A; Genebank
671 MF113386)[9]; NrHV-B (Genebank ON758386) and RHV-rn1 (Genebank KX905133)[36] as
672 outgroups. **(B)** Non-synonymous/synonymous (dN/dS) mutation ratios. Using whole
673 ORF sequencing data from (A), dN/dS ratios were generated for each viral protein.
674 Increased dN/dS is associated with increased evolutionary change.
675
676 **Figure S11. Liver pathology in mock and NrHV infected WT C57BL/6J mice.** Liver
677 tissue sections from mock or NrHV infected mice at 2, 7, 28 and 272 dpi were stained
678 with hematoxylin and eosin. Hallmark features of normal liver architecture including
679 portal vein, bile duct, hepatic artery, central vein and hepatocytes are noted in each
680 mock panel. Other pathologic features are noted in the key.
681
682 **Figure S12. Liver pathology in mock and NrHV infected CC046 mice.** Liver tissue
683 sections from mock or NrHV infected mice at 2, 7, 28 and 272 dpi were stained with
684 hematoxylin and eosin. Hallmark features of normal liver architecture including portal
685 vein, bile duct, hepatic artery, central vein and hepatocytes are noted in each mock
686 panel. Other pathologic features are noted in the key.
687
688 **Figure S13. Liver pathology in mock and NrHV infected CC071 mice.** Liver tissue
689 sections from mock or NrHV infected mice at 2, 7, 28 and 272 dpi were stained with

bioRxiv preprint doi: https://doi.org/10.1101/2023.03.18.533278; this version posted March 19, 2023. The copyright holder for this preprint (which was not certified by peer review) is the author/funder, who has granted bioRxiv a license to display the preprint in perpetuity. It is made available under aCC-BY-NC-ND 4.0 International license.

hematoxylin and eosin. Hallmark features of normal liver architecture including portal vein, bile duct, hepatic artery, central vein and hepatocytes are noted in each mock panel. Other pathologic features are noted in the key.

Figure S14. Liver pathology in mock and NrHV infected CC080 mice. Liver tissue sections from mock or NrHV infected mice at 2, 7, 28 and 272 dpi were stained with hematoxylin and eosin. Hallmark features of normal liver architecture including portal vein, bile duct, hepatic artery, central vein and hepatocytes are noted in each mock panel. Other pathologic features are noted in the key.

Figure S15. Summary of key phenotypic data per mouse strain. Key phenotypic data per mouse strain is shown to provide an overview of the main pieces of data described in the manuscript.

References

1. Li DK, Chung RT. Impact of hepatitis C virus eradication on hepatocellular carcinogenesis. *Cancer.* 2015;121(17):2874-2882.
2. Martinello M, Hajarizadeh B, Grebely J, Dore GJ, Matthews GV. Management of acute HCV infection in the era of direct-acting antiviral therapy. *Nat Rev Gastroenterol Hepatol.* 2018;15(7):412-424.
3. Villanueva A, Hernandez-Gea V, Llovet JM. Medical therapies for hepatocellular carcinoma: a critical view of the evidence. *Nat Rev Gastroenterol Hepatol.* 2013;10(1):34-42.

bioRxiv preprint doi: https://doi.org/10.1101/2023.03.18.533278; this version posted March 19, 2023. The copyright holder for this preprint (which was not certified by peer review) is the author/funder, who has granted bioRxiv a license to display the preprint in perpetuity. It is made available under aCC-BY-NC-ND 4.0 International license.

4. Zoulim F, Liang TJ, Gerbes AL, Aghemo A, Deuffic-Burban S, Dusheiko G, Fried MW, Pol S, Rockstroh JK, Terrault NA, Wiktor S. Hepatitis C virus treatment in the real world: optimising treatment and access to therapies. *Gut.* 2015;64(11):1824-1833.
5. Walker CM, Grakoui A. Hepatitis C virus: why do we need a vaccine to prevent a curable persistent infection? *Curr Opin Immunol.* 2015;35:137-143.
6. Gauthiez E, Habfast-Robertson I, Rueger S, Kutalik Z, Aubert V, Berg T, Cerny A, Gorgievski M, George J, Heim MH, Malinverni R, Moradpour D, Mullhaupt B, Negro F, Semela D, Semmo N, Villard J, Bibert S, Bochud PY, Swiss Hepatitis CCS. A systematic review and meta-analysis of HCV clearance. *Liver Int.* 2017;37(10):1431-1445.
7. Scheel TK, Simmonds P, Kapoor A. Surveying the global virome: identification and characterization of HCV-related animal hepaciviruses. *Antiviral Res.* 2015;115:83-93.
8. Firth C, Bhat M, Firth MA, Williams SH, Frye MJ, Simmonds P, Conte JM, Ng J, Garcia J, Bhuva NP, Lee B, Che X, Quan PL, Lipkin WI. Detection of zoonotic pathogens and characterization of novel viruses carried by commensal Rattus norvegicus in New York City. *MBio.* 2014;5(5):e01933-01914.
9. Billerbeck E, Wolfisberg R, Fahnoe U, Xiao JW, Quirk C, Luna JM, Cullen JM, Hartlage AS, Chiriboga L, Ghoshal K, Lipkin WI, Bukh J, Scheel TKH, Kapoor A, Rice CM. Mouse models of acute and chronic hepacivirus infection. *Science.* 2017;357(6347):204-208.
10. Wolfisberg R, Thorselius CE, Salinas E, Elrod E, Trivedi S, Nielsen L, Fahnoe U, Kapoor A, Grakoui A, Rice CM, Bukh J, Holmbeck K, Scheel TKH. Neutralization and receptor use of infectious culture-derived rat hepacivirus as a model for HCV. *Hepatology.* 2022.
11. Wolfisberg R, Holmbeck K, Nielsen L, Kapoor A, Rice CM, Bukh J, Scheel TKH. Replicons of a Rodent Hepatitis C Model Virus Permit Selection of Highly Permissive Cells. *J Virol.* 2019;93(19).
12. Threadgill DW, Miller DR, Churchill GA, de Villena FP. The collaborative cross: a recombinant inbred mouse population for the systems genetic era. *ILAR J.* 2011;52(1):24-31.
13. Noll KE, Ferris MT, Heise MT. The Collaborative Cross: A Systems Genetics Resource for Studying Host-Pathogen Interactions. *Cell Host Microbe.* 2019;25(4):484-498.
14. Srivastava A, Morgan AP, Najarian ML, Sarsani VK, Sigmon JS, Shorter JR, Kashfeen A, McMullan RC, Williams LH, Giusti-Rodriguez P, Ferris MT, Sullivan P, Hock P, Miller DR, Bell TA, McMillan L, Churchill GA, de Villena FP. Genomes of the Mouse Collaborative Cross. *Genetics.* 2017;206(2):537-556.
15. Rasmussen AL, Okumura A, Ferris MT, Green R, Feldmann F, Kelly SM, Scott DP, Safronetz D, Haddock E, LaCasse R, Thomas MJ, Sova P, Carter VS, Weiss JM, Miller DR, Shaw GD, Korth MJ, Heise MT, Baric RS, de Villena FP, Feldmann H, Katze MG. Host genetic diversity enables Ebola hemorrhagic fever pathogenesis and resistance. *Science.* 2014;346(6212):987-991.
16. Gralinski LE, Menachery VD, Morgan AP, Totura AL, Beall A, Kocher J, Plante J, Harrison-Shostak DC, Schafer A, Pardo-Manuel de Villena F, Ferris MT, Baric

bioRxiv preprint doi: https://doi.org/10.1101/2023.03.18.533278; this version posted March 19, 2023. The copyright holder for this preprint (which was not certified by peer review) is the author/funder, who has granted bioRxiv a license to display the preprint in perpetuity. It is made available under aCC-BY-NC-ND 4.0 International license.

RS. Allelic Variation in the Toll-Like Receptor Adaptor Protein Ticam2 Contributes to SARS-Coronavirus Pathogenesis in Mice. *G3 (Bethesda).* 2017;7(6):1653-1663.

17. Graham JB, Swarts JL, Wilkins C, Thomas S, Green R, Sekine A, Voss KM, Ireton RC, Mooney M, Choonoo G, Miller DR, Treuting PM, Pardo Manuel de Villena F, Ferris MT, McWeeney S, Gale M, Jr., Lund JM. A Mouse Model of Chronic West Nile Virus Disease. *PLoS Pathog.* 2016;12(11):e1005996.
18. Graham JB, Thomas S, Swarts J, McMillan AA, Ferris MT, Suthar MS, Treuting PM, Ireton R, Gale M, Jr., Lund JM. Genetic diversity in the collaborative cross model recapitulates human West Nile virus disease outcomes. *MBio.* 2015;6(3):e00493-00415.
19. Schafer A, Leist SR, Gralinski LE, Martinez DR, Winkler ES, Okuda K, Hawkins PE, Gully KL, Graham RL, Scobey DT, Bell TA, Hock P, Shaw GD, Loome JF, Madden EA, Anderson E, Baxter VK, Taft-Benz SA, Zweigart MR, May SR, Dong S, Clark M, Miller DR, Lynch RM, Heise MT, Tisch R, Boucher RC, Pardo Manuel de Villena F, Montgomery SA, Diamond MS, Ferris MT, Baric RS. A Multitrait Locus Regulates Sarbecovirus Pathogenesis. *mBio.* 2022;13(4):e0145422.
20. Ferris MT, Aylor DL, Bottomly D, Whitmore AC, Aicher LD, Bell TA, Bradel-Tretheway B, Bryan JT, Buus RJ, Gralinski LE, Haagmans BL, McMillan L, Miller DR, Rosenzweig E, Valdar W, Wang J, Churchill GA, Threadgill DW, McWeeney SK, Katze MG, Pardo-Manuel de Villena F, Baric RS, Heise MT. Modeling host genetic regulation of influenza pathogenesis in the collaborative cross. *PLoS Pathog.* 2013;9(2):e1003196.
21. Hartlage AS, Walker CM, Kapoor A. Priming of Antiviral CD8 T Cells without Effector Function by a Persistently Replicating Hepatitis C-Like Virus. *J Virol.* 2020;94(10).
22. Schwertheim S, Kalsch J, Jastrow H, Schaefer CM, Theurer S, Ting S, Canbay A, Wedemeyer H, Schmid KW, Baba HA. Characterization of two types of intranuclear hepatocellular inclusions in NAFLD. *Sci Rep.* 2020;10(1):16533.
23. Schwertheim S, Westerwick D, Jastrow H, Theurer S, Schaefer CM, Kalsch J, Mollmann D, Schlattjan M, Wedemeyer H, Schmid KW, Baba HA. Intranuclear inclusions in hepatocellular carcinoma contain autophagy-associated proteins and correlate with prolonged survival. *J Pathol Clin Res.* 2019;5(3):164-176.
24. Thongthip S, Bellani M, Gregg SQ, Sridhar S, Conti BA, Chen Y, Seidman MM, Smogorzewska A. Fan1 deficiency results in DNA interstrand cross-link repair defects, enhanced tissue karyomegaly, and organ dysfunction. *Genes Dev.* 2016;30(6):645-659.
25. Pawlotsky JM, Feld JJ, Zeuzem S, Hoofnagle JH. From non-A, non-B hepatitis to hepatitis C virus cure. *J Hepatol.* 2015;62(1 Suppl):S87-99.
26. Burke KP, Cox AL. Hepatitis C virus evasion of adaptive immune responses: a model for viral persistence. *Immunol Res.* 2010;47(1-3):216-227.
27. Prokunina-Olsson L, Muchmore B, Tang W, Pfeiffer RM, Park H, Dickensheets H, Hergott D, Porter-Gill P, Mumy A, Kohaar I, Chen S, Brand N, Tarway M, Liu L, Sheikh F, Astemborski J, Bonkovsky HL, Edlin BR, Howell CD, Morgan TR, Thomas DL, Rehermann B, Donnelly RP, O'Brien TR. A variant upstream of

bioRxiv preprint doi: https://doi.org/10.1101/2023.03.18.533278; this version posted March 19, 2023. The copyright holder for this preprint (which was not certified by peer review) is the author/funder, who has granted bioRxiv a license to display the preprint in perpetuity. It is made available under aCC-BY-NC-ND 4.0 International license.

IFNL3 (IL28B) creating a new interferon gene IFNL4 is associated with impaired clearance of hepatitis C virus. *Nature genetics.* 2013;45(2):164-171.

28. Thomas DL, Thio CL, Martin MP, Qi Y, Ge D, O'Huigin C, Kidd J, Kidd K, Khakoo SI, Alexander G, Goedert JJ, Kirk GD, Donfield SM, Rosen HR, Tobler LH, Busch MP, McHutchison JG, Goldstein DB, Carrington M. Genetic variation in IL28B and spontaneous clearance of hepatitis C virus. *Nature.* 2009;461(7265):798-801.
29. Urban TJ, Thompson AJ, Bradrick SS, Fellay J, Schuppan D, Cronin KD, Hong L, McKenzie A, Patel K, Shianna KV, McHutchison JG, Goldstein DB, Afdhal N. IL28B genotype is associated with differential expression of intrahepatic interferon-stimulated genes in patients with chronic hepatitis C. *Hepatology.* 2010;52(6):1888-1896.
30. Heim MH, Thimme R. Innate and adaptive immune responses in HCV infections. *J Hepatol.* 2014;61(1 Suppl):S14-25.
31. Cartwright HN, Barbeau DJ, Doyle JD, Klein E, Heise MT, Ferris MT, McElroy AK. Genetic diversity of collaborative cross mice enables identification of novel rift valley fever virus encephalitis model. *PLoS Pathog.* 2022;18(7):e1010649.
32. Manet C, Simon-Loriere E, Jouvion G, Hardy D, Prot M, Conquet L, Flamand M, Panthier JJ, Sakuntabhai A, Montagutelli X. Genetic Diversity of Collaborative Cross Mice Controls Viral Replication, Clinical Severity, and Brain Pathology Induced by Zika Virus Infection, Independently of Oas1b. *J Virol.* 2020;94(3).
33. Jasperse BA, Mattocks MD, Noll KM, Ferris MT, Heise MT, Lazear HM. Neuroinvasive flavivirus pathogenesis is restricted by host genetic factors in Collaborative Cross mice, independently of Oas1b. *bioRxiv.* 2022:2022.2010.2024.513634.
34. Zhang J, Malo D, Mott R, Panthier JJ, Montagutelli X, Jaubert J. Identification of new loci involved in the host susceptibility to Salmonella Typhimurium in collaborative cross mice. *BMC Genomics.* 2018;19(1):303.
35. Bukh J. Animal models for the study of hepatitis C virus infection and related liver disease. *Gastroenterology.* 2012;142(6):1279-1287 e1273.
36. Trivedi S, Murthy S, Sharma H, Hartlage AS, Kumar A, Gadi SV, Simmonds P, Chauhan LV, Scheel TKH, Billerbeck E, Burbelo PD, Rice CM, Lipkin WI, Vandegrift K, Cullen JM, Kapoor A. Viral persistence, liver disease, and host response in a hepatitis C-like virus rat model. *Hepatology.* 2018;68(2):435-448.
37. Welsh CE, Miller DR, Manly KF, Wang J, McMillan L, Morahan G, Mott R, Iraqi FA, Threadgill DW, de Villena FP. Status and access to the Collaborative Cross population. *Mamm Genome.* 2012;23(9-10):706-712.
38. Livak KJ, Schmittgen TD. Analysis of relative gene expression data using real-time quantitative PCR and the 2(-Delta Delta C(T)) Method. *Methods.* 2001;25(4):402-408.
39. Fahnoe U, Pedersen AG, Johnston CM, Orton RJ, Hoper D, Beer M, Bukh J, Belsham GJ, Rasmussen TB. Virus Adaptation and Selection Following Challenge of Animals Vaccinated against Classical Swine Fever Virus. *Viruses.* 2019;11(10).

bioRxiv preprint doi: https://doi.org/10.1101/2023.03.18.533278; this version posted March 19, 2023. The copyright holder for this preprint (which was not certified by peer review) is the author/funder, who has granted bioRxiv a license to display the preprint in perpetuity. It is made available under aCC-BY-NC-ND 4.0 International license.

852 40. Leist SR, Baric RS. Giving the Genes a Shuffle: Using Natural Variation to
853 Understand Host Genetic Contributions to Viral Infections. *Trends Genet.*
854 2018;34(10):777-789.
855

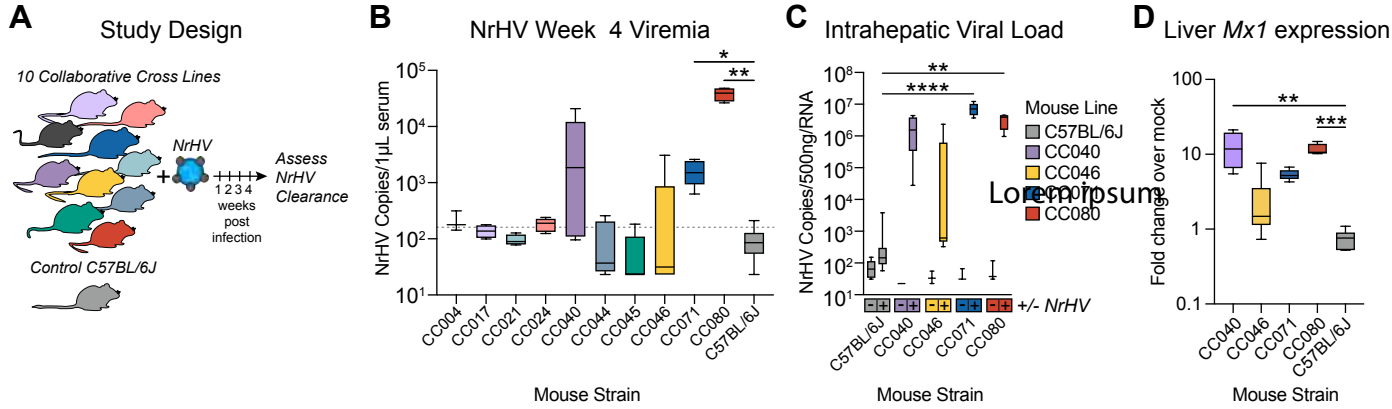

Lorem ipsum

Figure 1

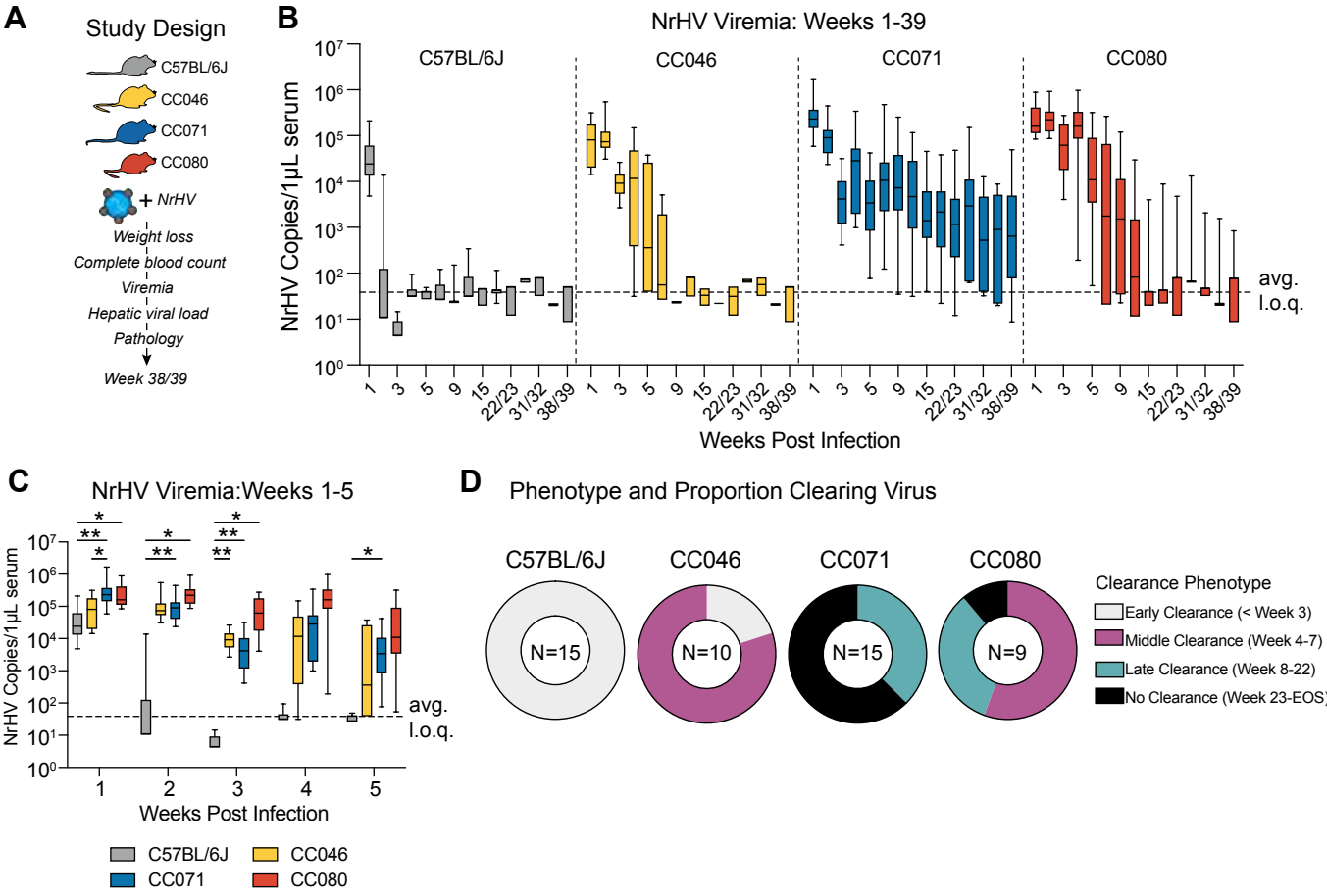
A
Study Design
C57BL/6J
CC046
CC071
CC080
+ NrHV
Weight loss
Complete blood count
Viremia
Hepatic viral load
Pathology
Week 38/39
B
NrHV Viremia: Weeks 1-39
C57BL/6J
CC046
CC071
CC080
NrHV Copies/1µL serum
avg. l.o.q.
Weeks Post Infection
C
NrHV Viremia:Weeks 1-5
NrHV Copies/1µL serum
avg. l.o.q.
Weeks Post Infection
C57BL/6J
CC046
CC071
CC080
D
Phenotype and Proportion Clearing Virus
C57BL/6J
CC046
CC071
CC080
N=15
N=10
N=15
N=9
Clearance Phenotype
Early Clearance (< Week 3)
Middle Clearance (Week 4-7)
Late Clearance (Week 8-22)
No Clearance (Week 23-EOS)

Figure 2

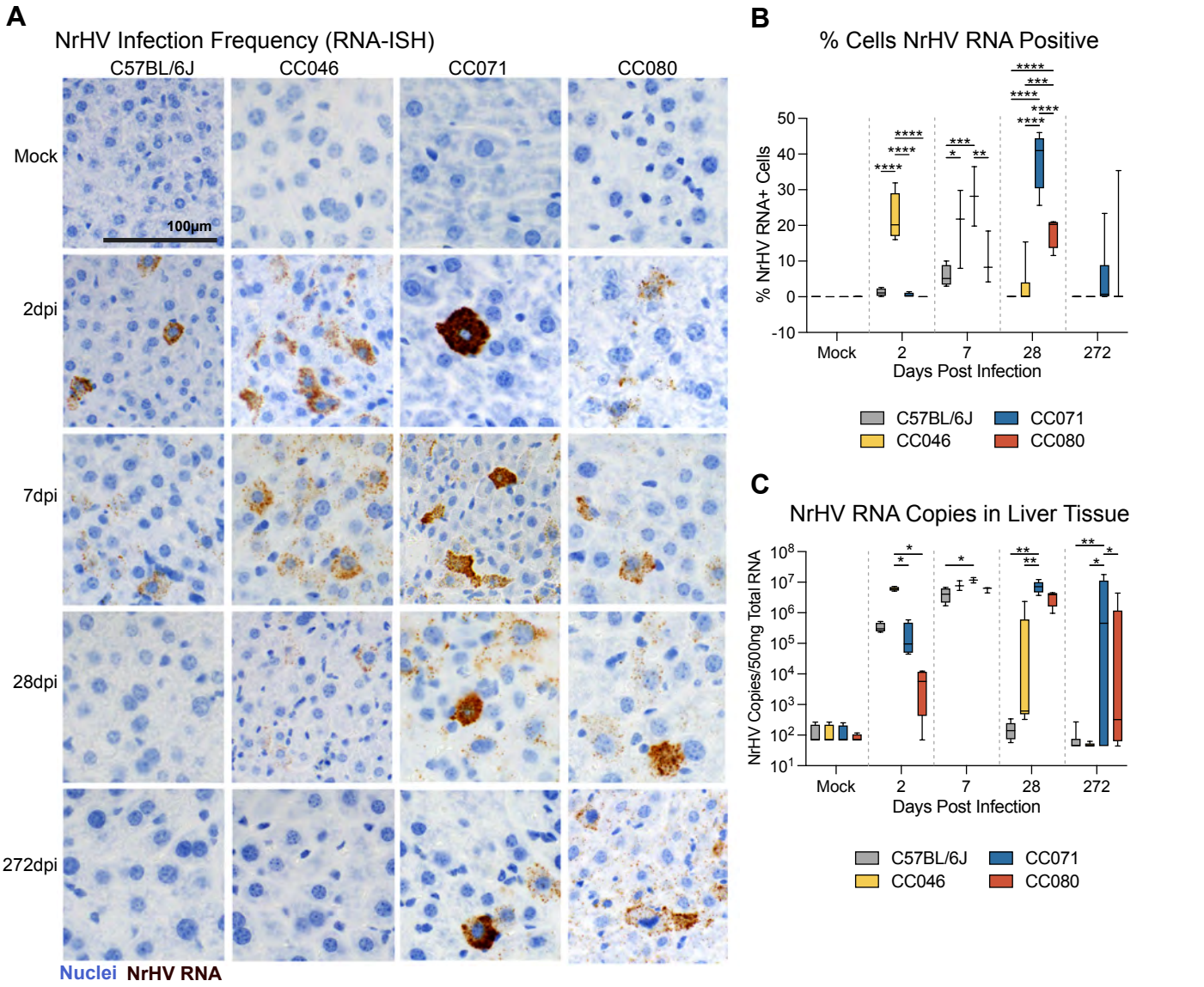
A
NrHV Infection Frequency (RNA-ISH)
C57BL/6J
CC046
CC071
CC080
Mock
2dpi
7dpi
28dpi
272dpi
100µm
Nuclei NrHV RNA
B
% Cells NrHV RNA Positive
% NrHV RNA+ Cells
Days Post Infection
Mock
2
7
28
272
C57BL/6J
CC046
CC071
CC080
C
NrHV RNA Copies in Liver Tissue
NrHV Copies/500ng Total RNA
Days Post Infection
C57BL/6J
CC046
CC071
CC080

Figure 3

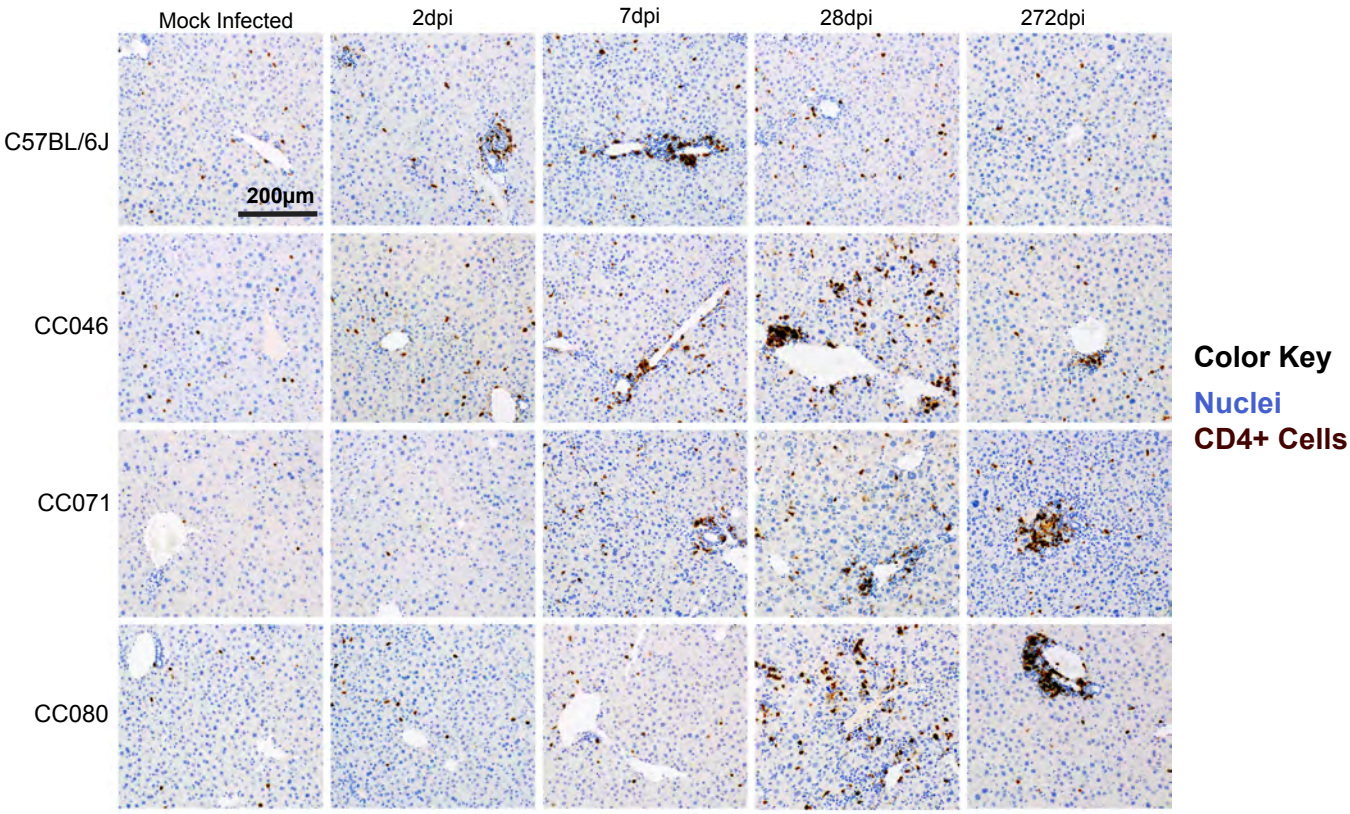
Mock Infected
2dpi
7dpi
28dpi
272dpi
C57BL/6J
CC046
CC071
CC080
200µm
Color Key
Nuclei
CD4+ Cells

Figure 4

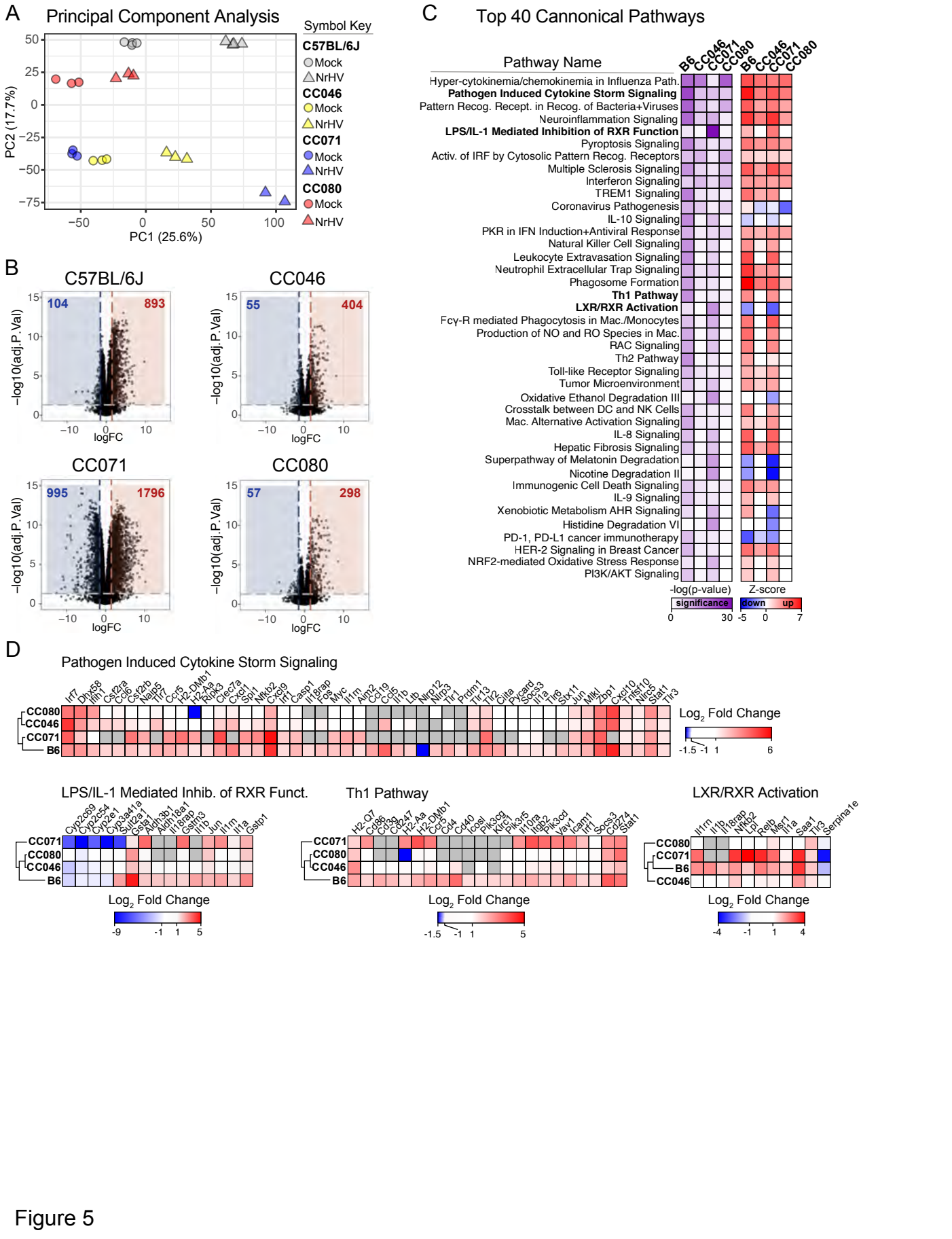
A
Principal Component Analysis
Symbol Key
C57BL/6J
Mock
NrHV
CC046
Mock
NrHV
CC071
Mock
NrHV
CC080
Mock
NrHV
PC2 (17.7%)
PC1 (25.6%)
B
C57BL/6J
CC046
CC071
CC080
104
893
55
404
995
1796
57
298
−log10(adj.P.Val)
logFC
C
Top 40 Cannonical Pathways
Pathway Name
B6
CC046
CC071
CC080
Hyper-cytokinemia/chemokinemia in Influenza Path.
Pathogen Induced Cytokine Storm Signaling
Pattern Recog. Recept. in Recog. of Bacteria+Viruses
Neuroinflammation Signaling
LPS/IL-1 Mediated Inhibition of RXR Function
Pyroptosis Signaling
Activ. of IRF by Cytosolic Pattern Recog. Receptors
Multiple Sclerosis Signaling
Interferon Signaling
TREM1 Signaling
Coronavirus Pathogenesis
IL-10 Signaling
PKR in IFN Induction+Antiviral Response
Natural Killer Cell Signaling
Leukocyte Extravasation Signaling
Neutrophil Extracellular Trap Signaling
Phagosome Formation
Th1 Pathway
LXR/RXR Activation
Fcγ-R mediated Phagocytosis in Mac./Monocytes
Production of NO and RO Species in Mac.
RAC Signaling
Th2 Pathway
Toll-like Receptor Signaling
Tumor Microenvironment
Oxidative Ethanol Degradation III
Crosstalk between DC and NK Cells
Mac. Alternative Activation Signaling
IL-8 Signaling
Hepatic Fibrosis Signaling
Superpathway of Melatonin Degradation
Nicotine Degradation II
Immunogenic Cell Death Signaling
IL-9 Signaling
Xenobiotic Metabolism AHR Signaling
Histidine Degradation VI
PD-1, PD-L1 cancer immunotherapy
HER-2 Signaling in Breast Cancer
NRF2-mediated Oxidative Stress Response
PI3K/AKT Signaling
-log(p-value)
significance
Z-score
down
up
D
Pathogen Induced Cytokine Storm Signaling
CC080
CC046
CC071
B6
Log2 Fold Change
LPS/IL-1 Mediated Inhib. of RXR Funct.
Th1 Pathway
LXR/RXR Activation

Figure 5

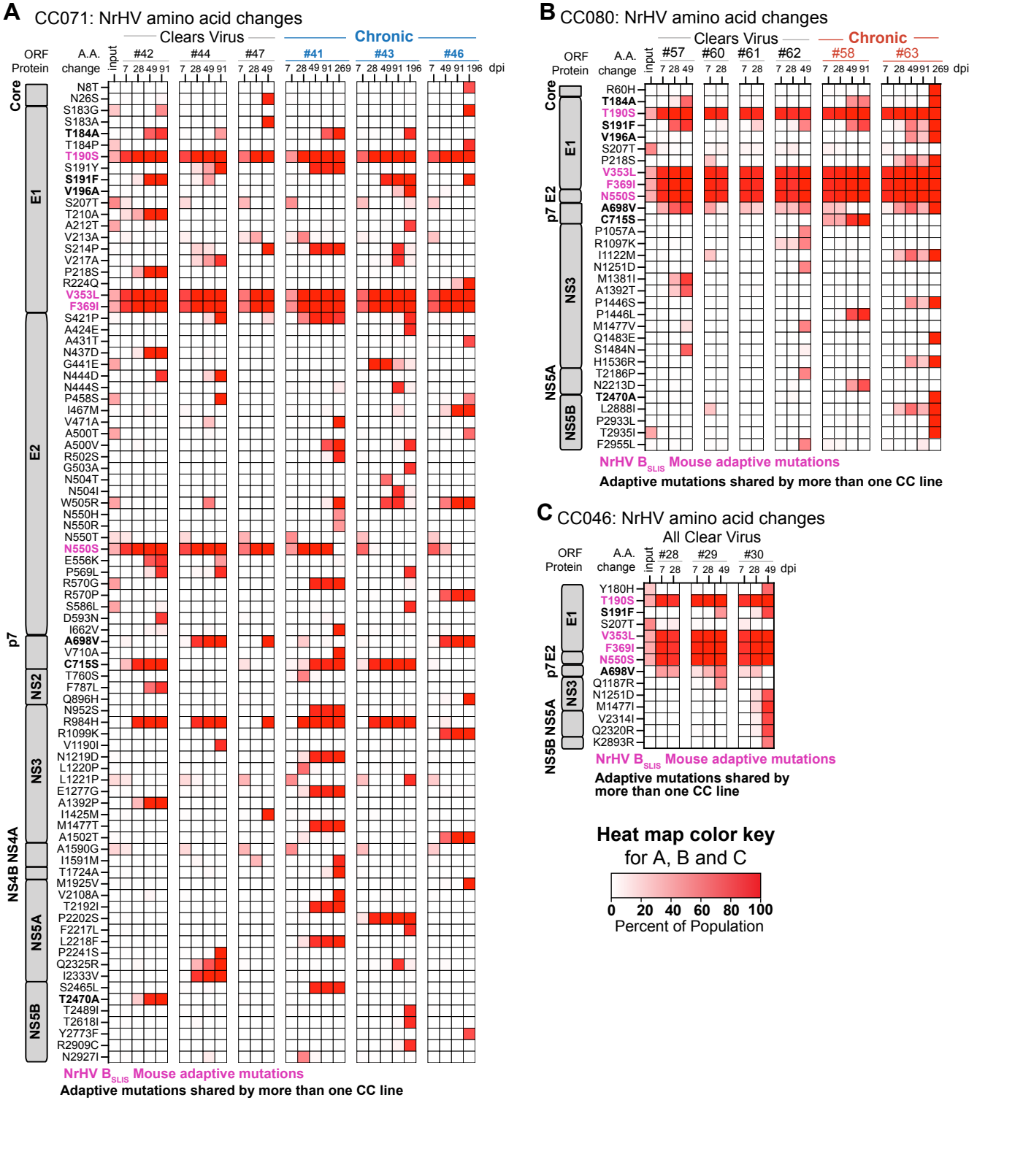
A
CC071: NrHV amino acid changes
Clears Virus
Chronic
ORF Protein
A.A. change
input
#42
#44
#47
#41
#43
#46
dpi
Core
E1
E2
p7
NS2
NS3
NS4A
NS4B
NS5A
NS5B
NrHV B SLIS Mouse adaptive mutations
Adaptive mutations shared by more than one CC line
B
CC080: NrHV amino acid changes
Clears Virus
Chronic
#57
#60
#61
#62
#58
#63
NrHV B SLIS Mouse adaptive mutations
Adaptive mutations shared by more than one CC line
C
CC046: NrHV amino acid changes
All Clear Virus
#28
#29
#30
NrHV B SLIS Mouse adaptive mutations
Adaptive mutations shared by more than one CC line
Heat map color key
for A, B and C
0 20 40 60 80 100
Percent of Population

Figure 6

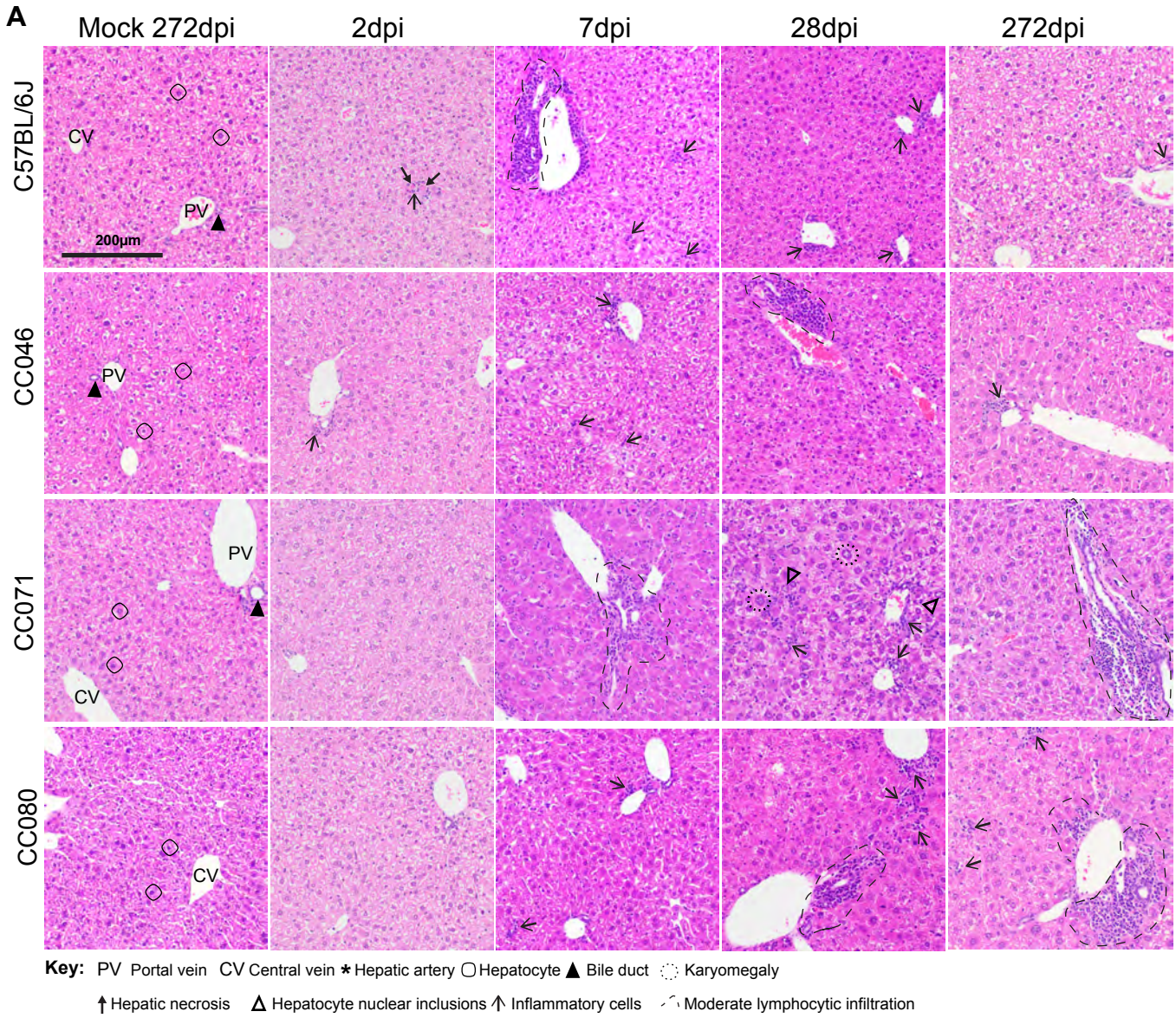

Key: PV Portal vein CV Central vein * Hepatic artery ○ Hepatocyte ▲ Bile duct ◌ Karyomegaly

↑ Hepatic necrosis △ Hepatocyte nuclear inclusions ↑ Inflammatory cells ◠ Moderate lymphocytic infiltration

Figure 7

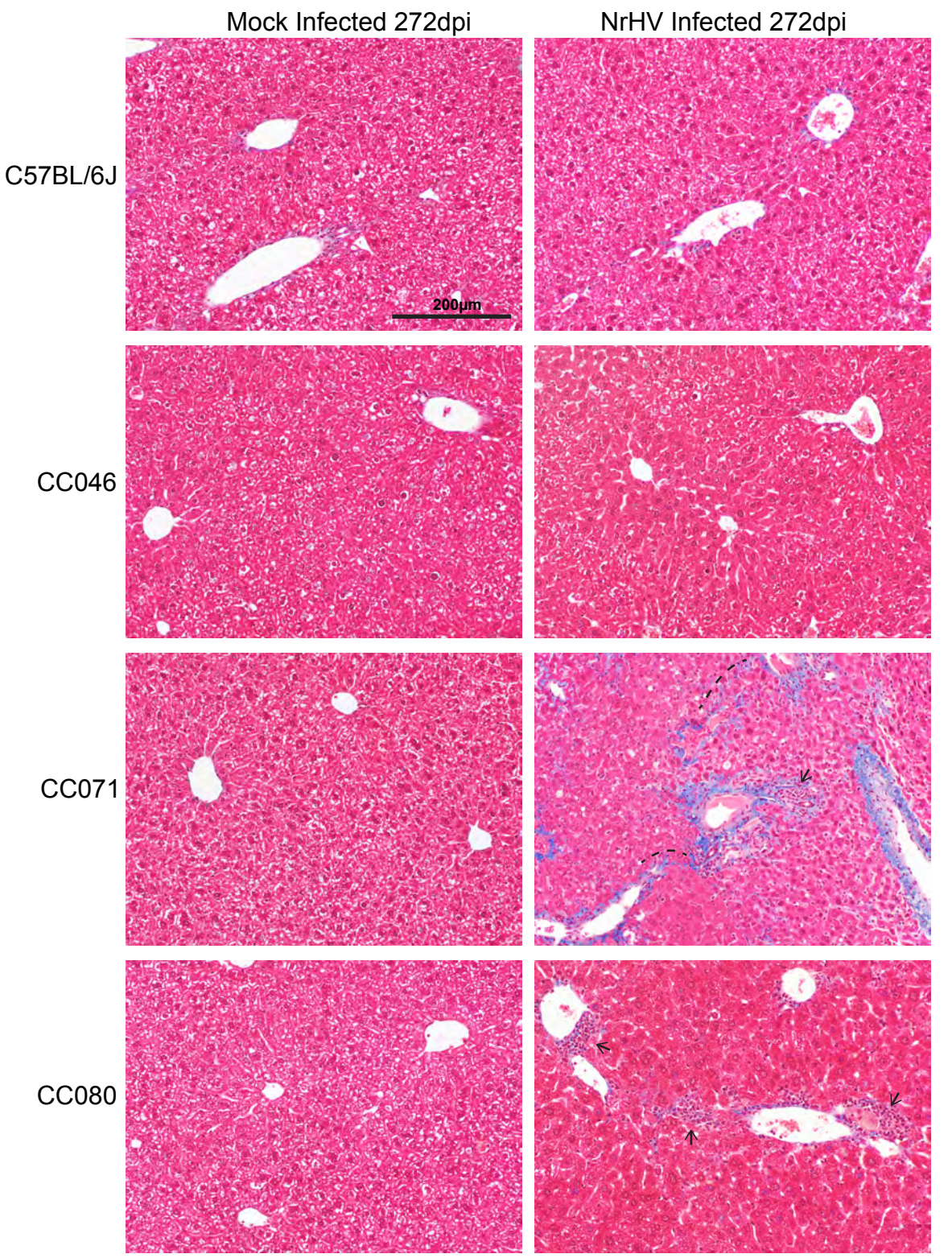
Mock Infected 272dpi
NrHV Infected 272dpi
C57BL/6J
CC046
CC071
CC080
200µm
Key: Collagen Cytoplasm Nuclei
Bridging Fibrosis
Inflammatory cells

Figure 8

A

Amino differences among recombinant input viruses

Pos.	Rn1	A	B	B_{SLIS}
180	Y	L	Y	Y
183	G	G	S	S
184	A	P	T	T
190	**T**	**T**	**T**	**S**
196	V	F	V	V
199	F	L	I	I
207	T	T	S	S
208	E	R	E	E
212	T	T	A	A
353	**V**	**V**	**V**	**L**
369	**F**	**F**	**F**	**I**
422	M	T	M	M
435	P	S	S	S
441	G	E	G	G
458	P	S	P	P
477	T	T	A	A
481	E	K	E	E
500	T	T	A	A
505	R	R	W	W
518	D	N	S	S
550	**N**	**N**	**N**	**S**
569	L	P	P	P
570	G	G	R	R
572	A	V	A	A
586	L	L	S	S
1397	V	A	V	V
1661	I	I	V	V
2213	D	N	N	N
2214	N	N	K	K
2223	E	E	V	V
2225	Q	R	R	R
2315	M	V	V	V
2575	R	Q	R	R
2586	K	K	N	N
2935	I	I	T	T

B

Deep sequencing of input populations

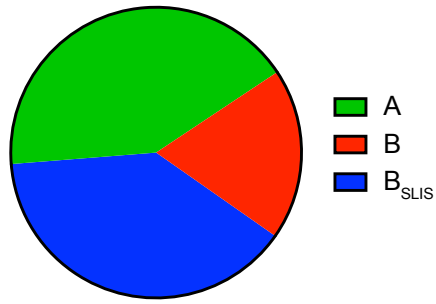

Figure S1

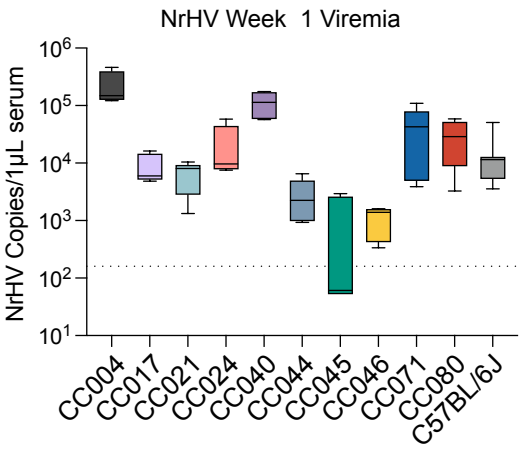
NrHV Week 1 Viremia
NrHV Copies/1µL serum
10^6
10^5
10^4
10^3
10^2
10^1
CC004
CC017
CC021
CC024
CC040
CC044
CC045
CC046
CC071
CC080
C57BL/6J

Figure S2

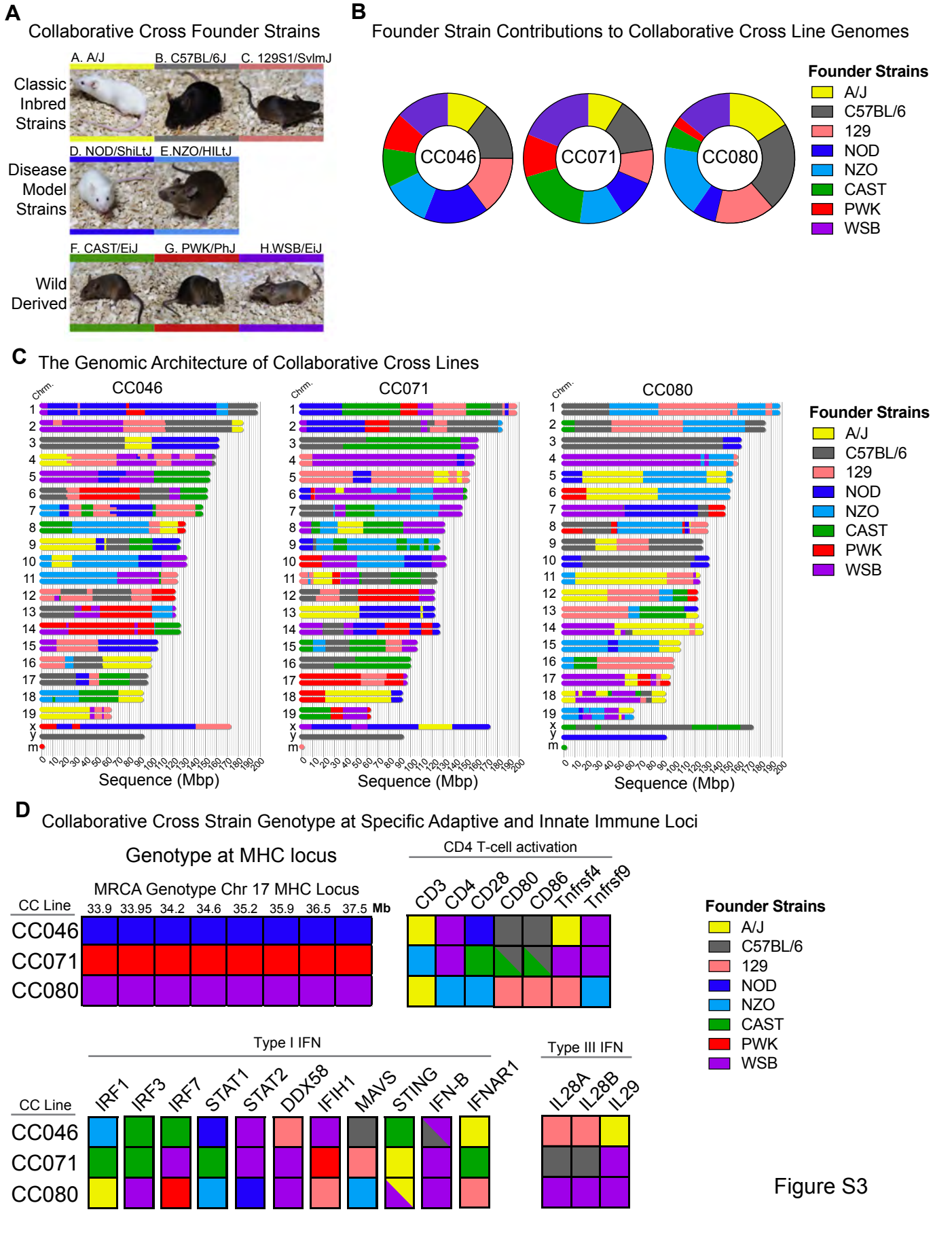
A
Collaborative Cross Founder Strains
A. A/J
B. C57BL/6J
C. 129S1/SvImJ
Classic Inbred Strains
D. NOD/ShiLtJ
E.NZO/HILtJ
Disease Model Strains
F. CAST/EiJ
G. PWK/PhJ
H.WSB/EiJ
Wild Derived
B
Founder Strain Contributions to Collaborative Cross Line Genomes
CC046
CC071
CC080
Founder Strains
A/J
C57BL/6
129
NOD
NZO
CAST
PWK
WSB
C
The Genomic Architecture of Collaborative Cross Lines
CC046
CC071
CC080
Chrm.
Sequence (Mbp)
D
Collaborative Cross Strain Genotype at Specific Adaptive and Innate Immune Loci
Genotype at MHC locus
MRCA Genotype Chr 17 MHC Locus
CC Line
33.9 33.95 34.2 34.6 35.2 35.9 36.5 37.5 Mb
CC046
CC071
CC080
CD4 T-cell activation
CD3
CD4
CD28
CD80
CD86
Tnfrsf4
Tnfrsf9
Type I IFN
IRF1
IRF3
IRF7
STAT1
STAT2
DDX58
IFIH1
MAVS
STING
IFN-B
IFNAR1
Type III IFN
IL28A
IL28B
IL29

Figure S3

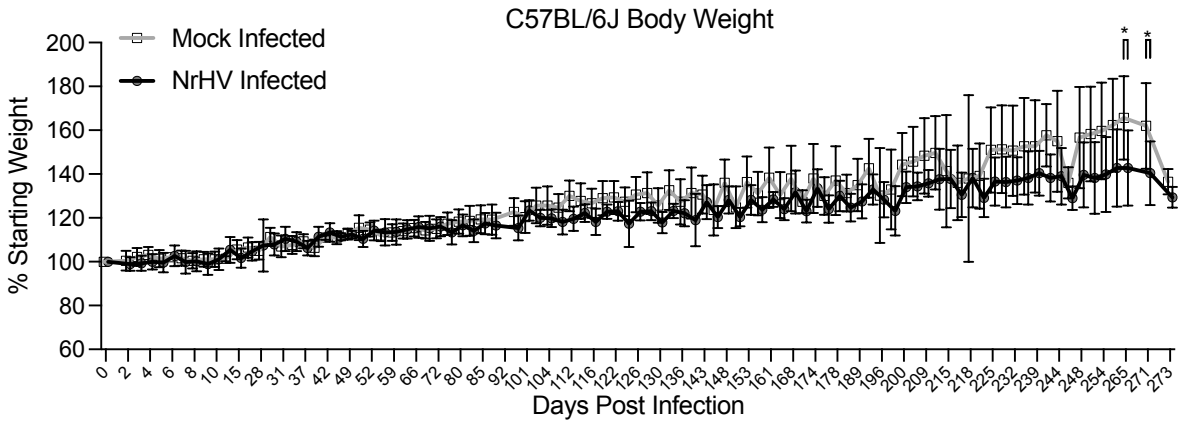
C57BL/6J Body Weight
Mock Infected
NrHV Infected
% Starting Weight
Days Post Infection

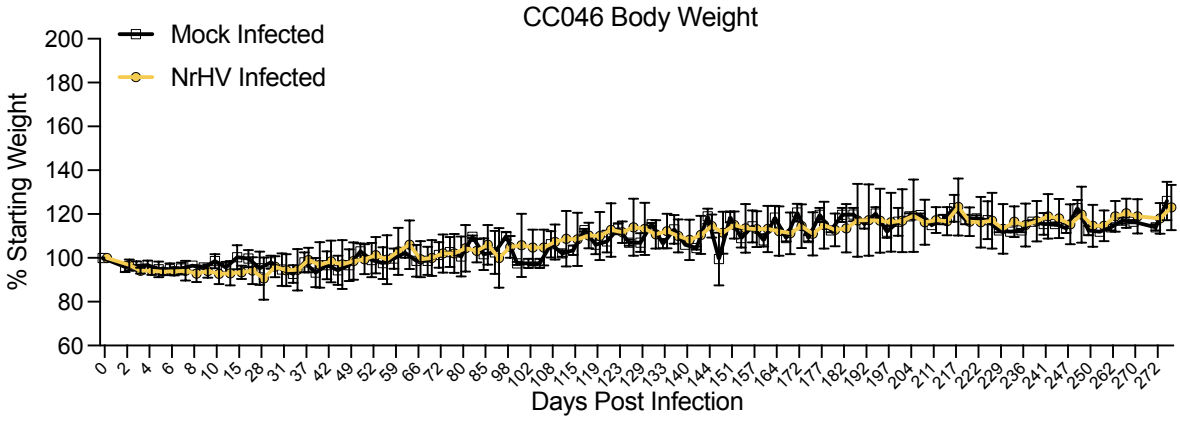
CC046 Body Weight
Mock Infected
NrHV Infected
% Starting Weight
Days Post Infection

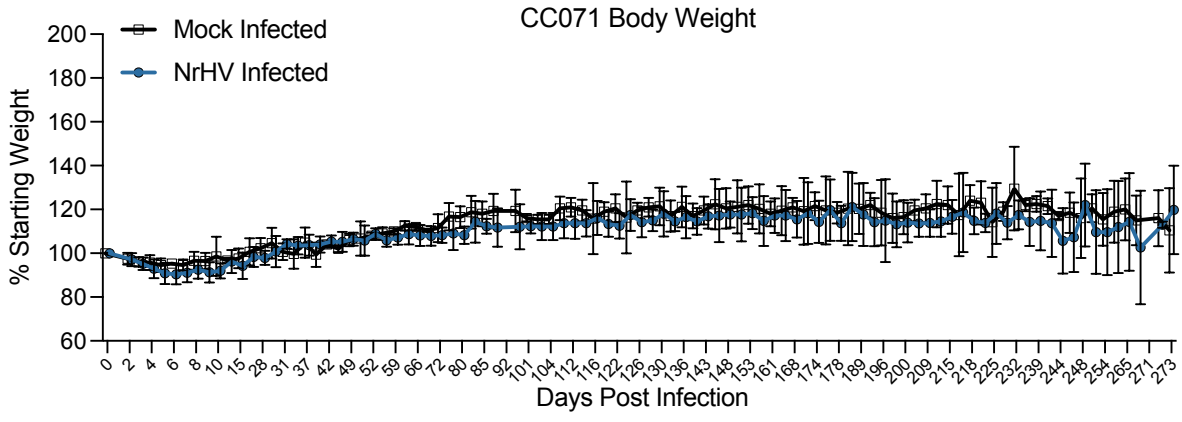
CC071 Body Weight
Mock Infected
NrHV Infected
% Starting Weight
Days Post Infection

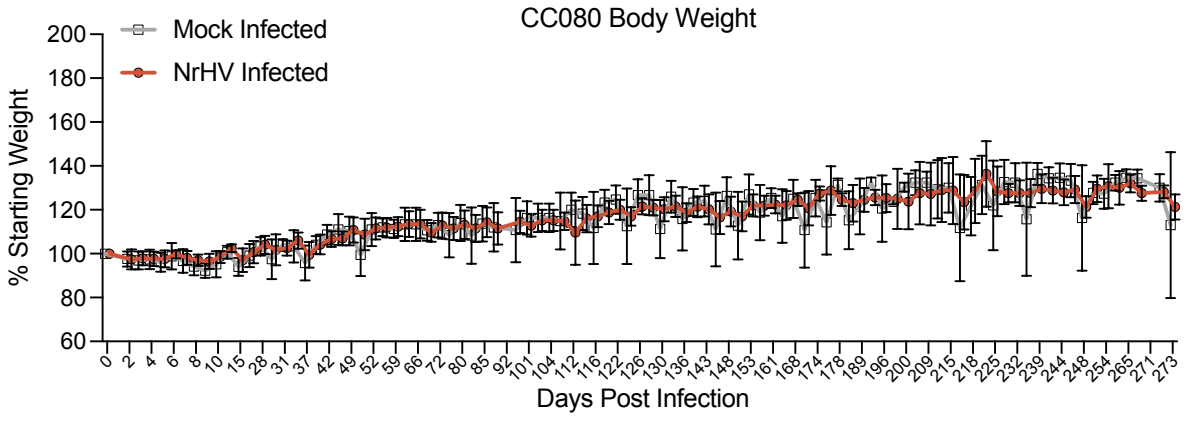
CC080 Body Weight
Mock Infected
NrHV Infected
% Starting Weight
Days Post Infection

Figure S4

Body Weight (Week 1-2)

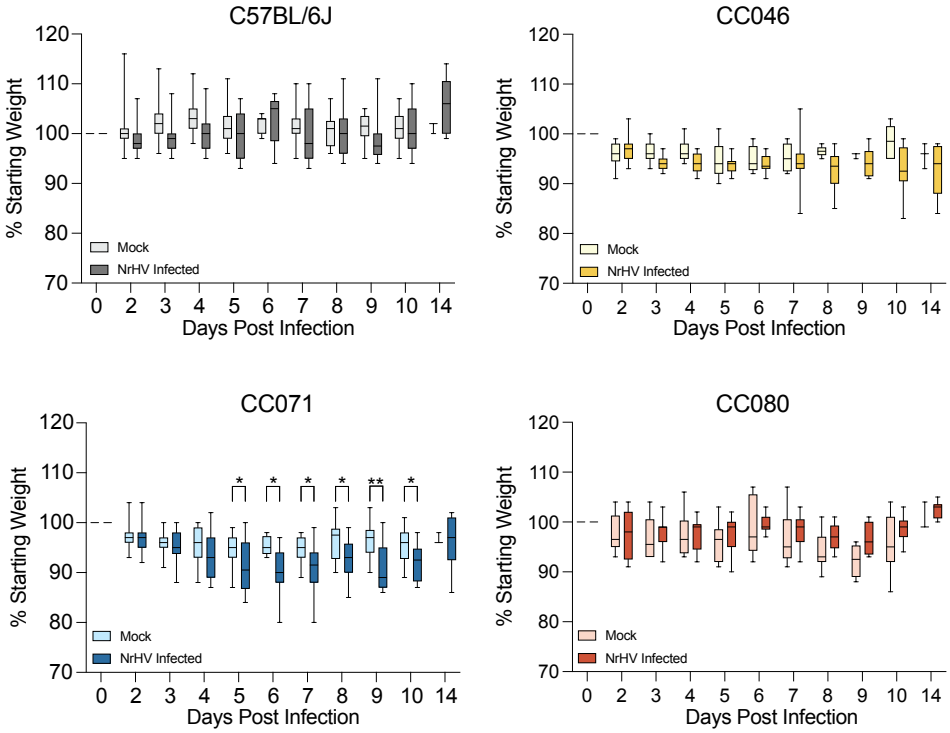

Figure S5

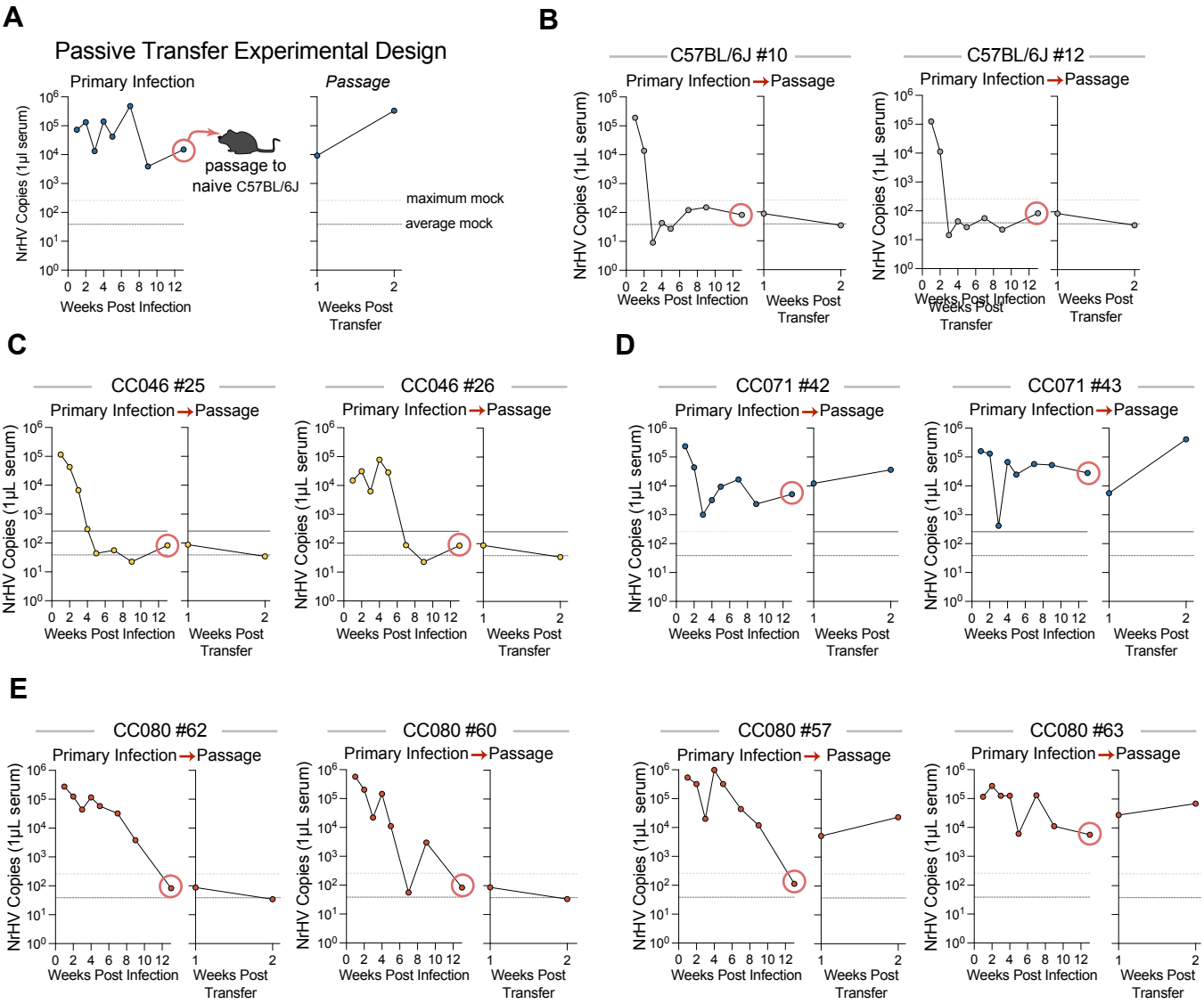
A
Passive Transfer Experimental Design
Primary Infection
Passage
NrHV Copies (1µl serum)
passage to
naive C57BL/6J
maximum mock
average mock
Weeks Post Infection
Weeks Post
Transfer
B
C57BL/6J #10
C57BL/6J #12
Primary Infection → Passage
NrHV Copies (1µL serum)
C
CC046 #25
CC046 #26
D
CC071 #42
CC071 #43
E
CC080 #62
CC080 #60
CC080 #57
CC080 #63

Figure S6

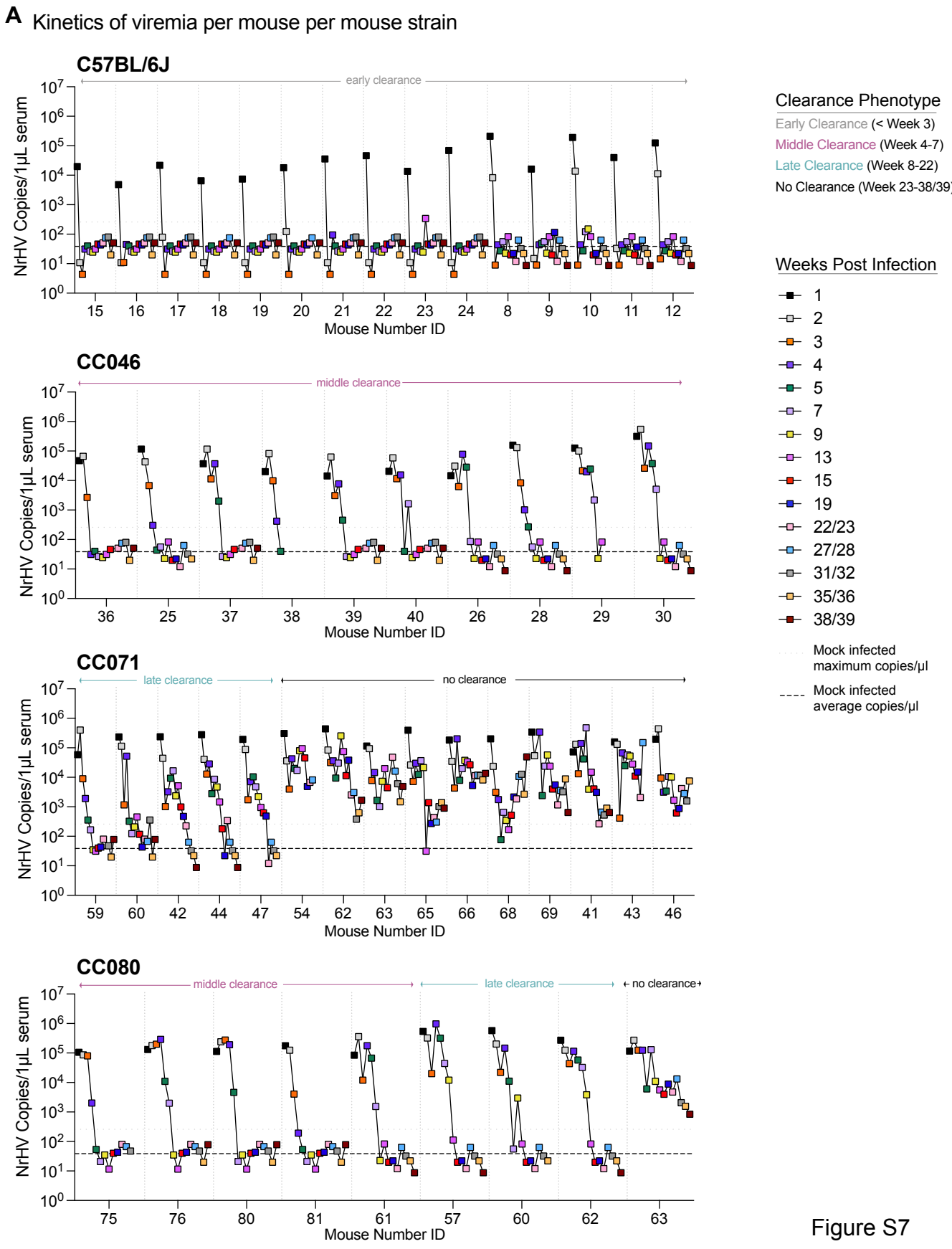
A
Kinetics of viremia per mouse per mouse strain
C57BL/6J
early clearance
NrHV Copies/1µL serum
Mouse Number ID
CC046
middle clearance
CC071
late clearance
no clearance
CC080
middle clearance
late clearance
no clearance
Clearance Phenotype
Early Clearance (< Week 3)
Middle Clearance (Week 4-7)
Late Clearance (Week 8-22)
No Clearance (Week 23-38/39)
Weeks Post Infection
1
2
3
4
5
7
9
13
15
19
22/23
27/28
31/32
35/36
38/39
Mock infected maximum copies/µl
Mock infected average copies/µl

Figure S7

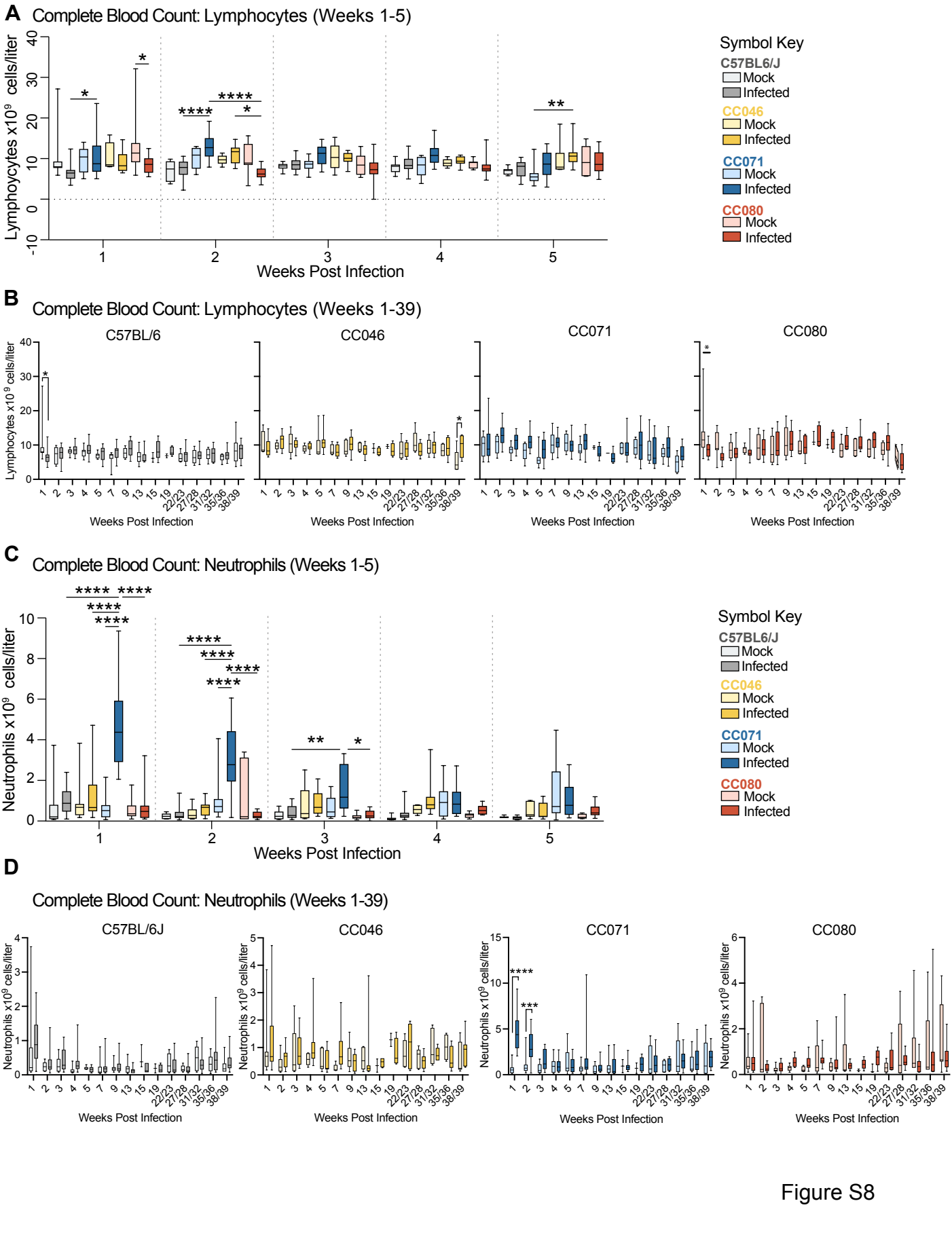
A
Complete Blood Count: Lymphocytes (Weeks 1-5)
Lymphocytes x10⁹ cells/liter
Weeks Post Infection
Symbol Key
C57BL6/J
Mock
Infected
CC046
Mock
Infected
CC071
Mock
Infected
CC080
Mock
Infected
B
Complete Blood Count: Lymphocytes (Weeks 1-39)
C57BL/6
CC046
CC071
CC080
Lymphocytes x10⁹ cells/liter
Weeks Post Infection
C
Complete Blood Count: Neutrophils (Weeks 1-5)
Neutrophils x10⁹ cells/liter
Weeks Post Infection
Symbol Key
C57BL6/J
Mock
Infected
CC046
Mock
Infected
CC071
Mock
Infected
CC080
Mock
Infected
D
Complete Blood Count: Neutrophils (Weeks 1-39)
C57BL/6J
CC046
CC071
CC080
Neutrophils x10⁹ cells/liter
Weeks Post Infection

Figure S8

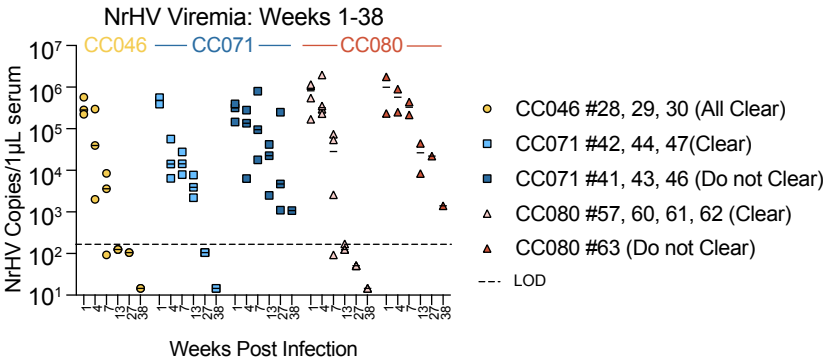
NrHV Viremia: Weeks 1-38
CC046
CC071
CC080
NrHV Copies/1µL serum
10^7
10^6
10^5
10^4
10^3
10^2
10^1
1
4
7
13
27
38
Weeks Post Infection
CC046 #28, 29, 30 (All Clear)
CC071 #42, 44, 47(Clear)
CC071 #41, 43, 46 (Do not Clear)
CC080 #57, 60, 61, 62 (Clear)
CC080 #63 (Do not Clear)
LOD

Figure S9

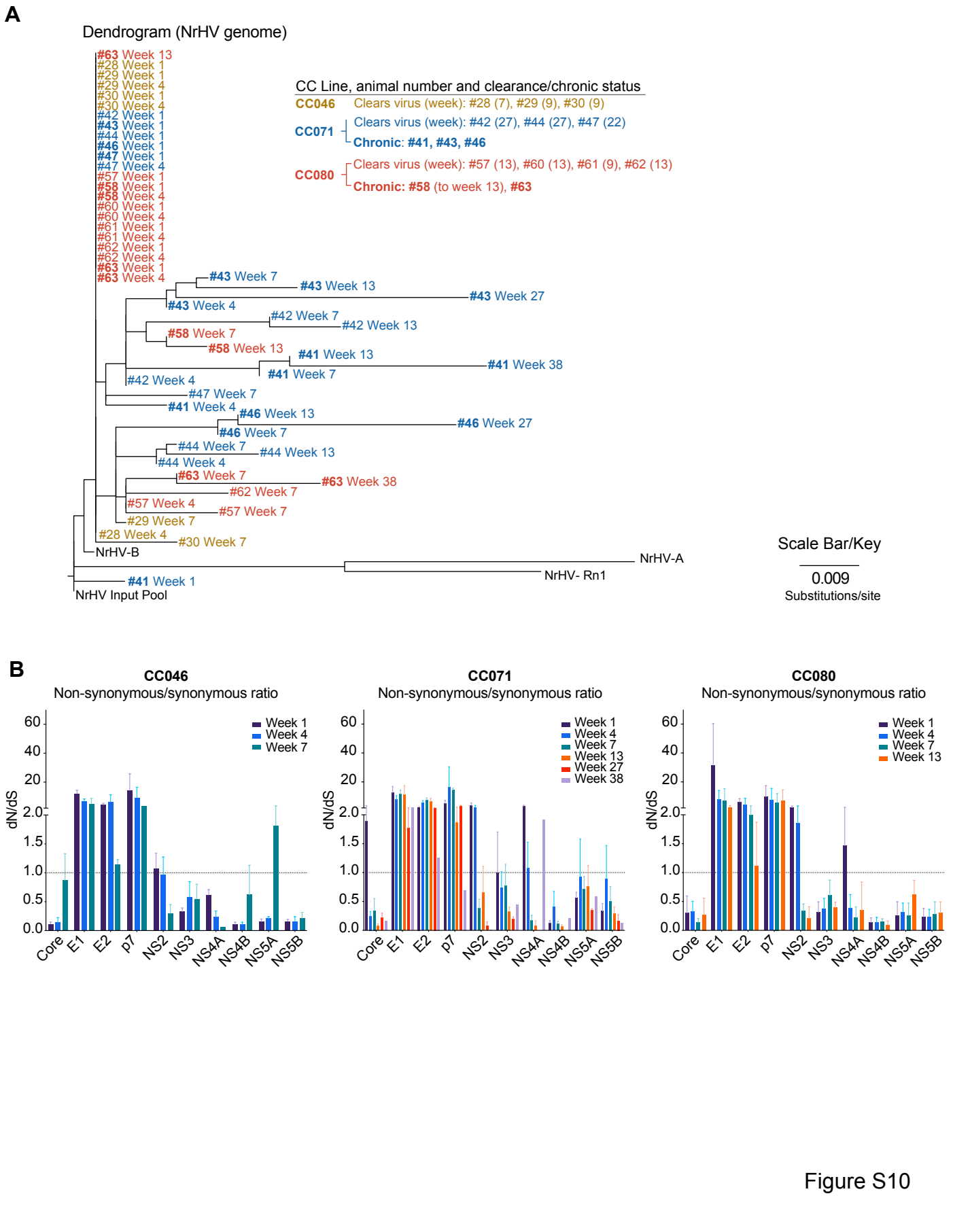
A
Dendrogram (NrHV genome)
#63 Week 13
#28 Week 1
#29 Week 1
#29 Week 4
#30 Week 1
#30 Week 4
#42 Week 1
#43 Week 1
#44 Week 1
#46 Week 1
#47 Week 1
#47 Week 4
#57 Week 1
#58 Week 1
#58 Week 4
#60 Week 1
#60 Week 4
#61 Week 1
#61 Week 4
#62 Week 1
#62 Week 4
#63 Week 1
#63 Week 4
CC Line, animal number and clearance/chronic status
CC046 Clears virus (week): #28 (7), #29 (9), #30 (9)
CC071 Clears virus (week): #42 (27), #44 (27), #47 (22)
Chronic: #41, #43, #46
CC080 Clears virus (week): #57 (13), #60 (13), #61 (9), #62 (13)
Chronic: #58 (to week 13), #63
#43 Week 7
#43 Week 13
#43 Week 27
#43 Week 4
#42 Week 7
#42 Week 13
#58 Week 7
#58 Week 13
#41 Week 13
#41 Week 38
#41 Week 7
#42 Week 4
#47 Week 7
#41 Week 4
#46 Week 13
#46 Week 27
#46 Week 7
#44 Week 7
#44 Week 13
#44 Week 4
#63 Week 7
#63 Week 38
#62 Week 7
#57 Week 4
#57 Week 7
#29 Week 7
#28 Week 4
#30 Week 7
NrHV-B
NrHV-A
NrHV- Rn1
#41 Week 1
NrHV Input Pool
Scale Bar/Key
0.009
Substitutions/site
B
CC046
Non-synonymous/synonymous ratio
CC071
Non-synonymous/synonymous ratio
CC080
Non-synonymous/synonymous ratio
dN/dS
Week 1
Week 4
Week 7
Week 13
Week 27
Week 38
Core
E1
E2
p7
NS2
NS3
NS4A
NS4B
NS5A
NS5B

Figure S10

C57BL/6J

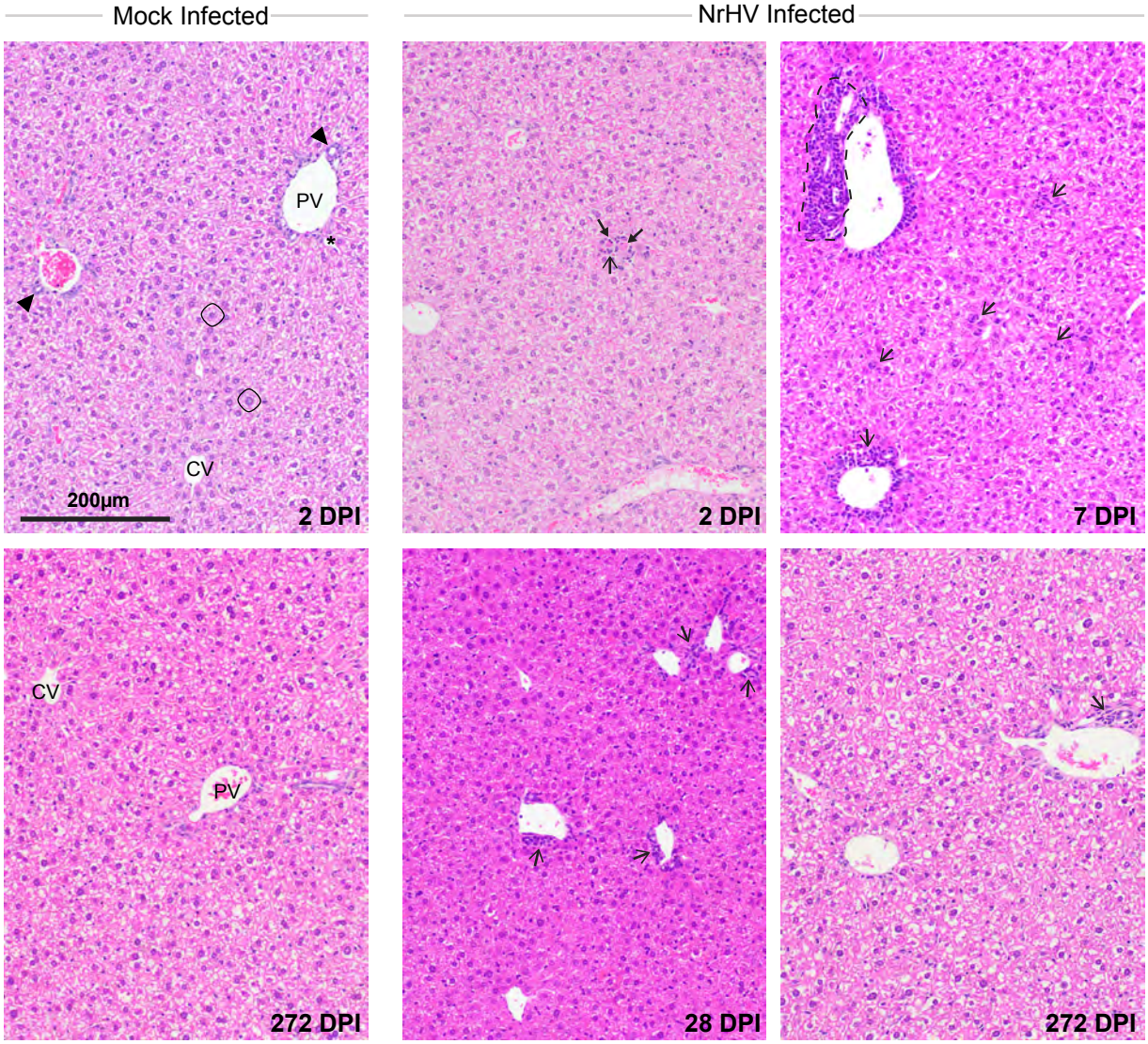

Key: PV Portal vein CV Central vein ○ Hepatocyte ▲ Bile duct

↑ Hepatic necrosis ↑ Inflammatory cells Moderate lymphocytic infiltration

Figure S11

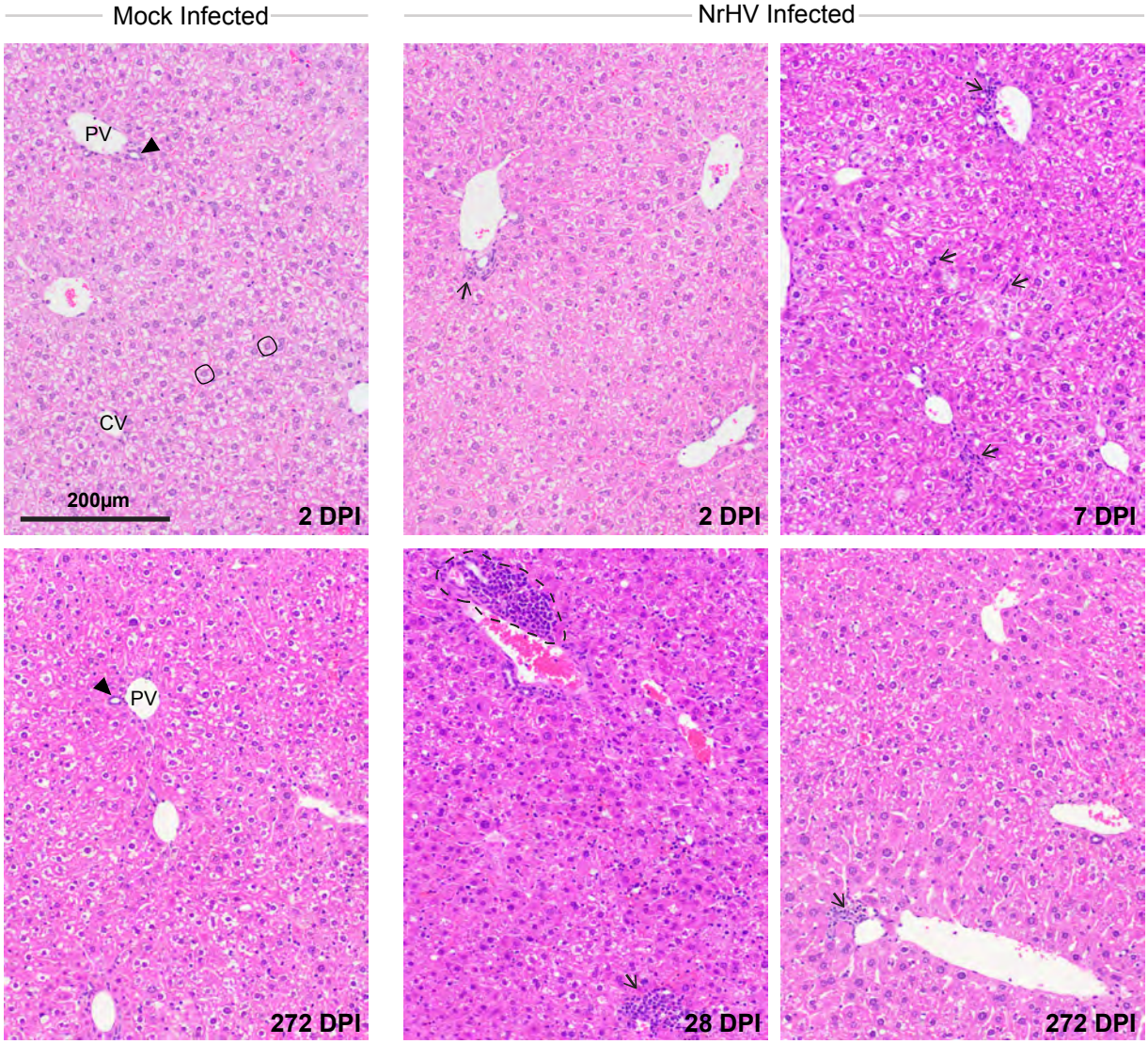
Mock Infected
NrHV Infected
PV
CV
200µm
2 DPI
2 DPI
7 DPI
PV
272 DPI
28 DPI
272 DPI
Key: PV Portal vein CV Central vein Hepatocyte Bile duct
Hepatic necrosis Inflammatory cells Moderate lymphocytic infiltration

Figure S12

CC071

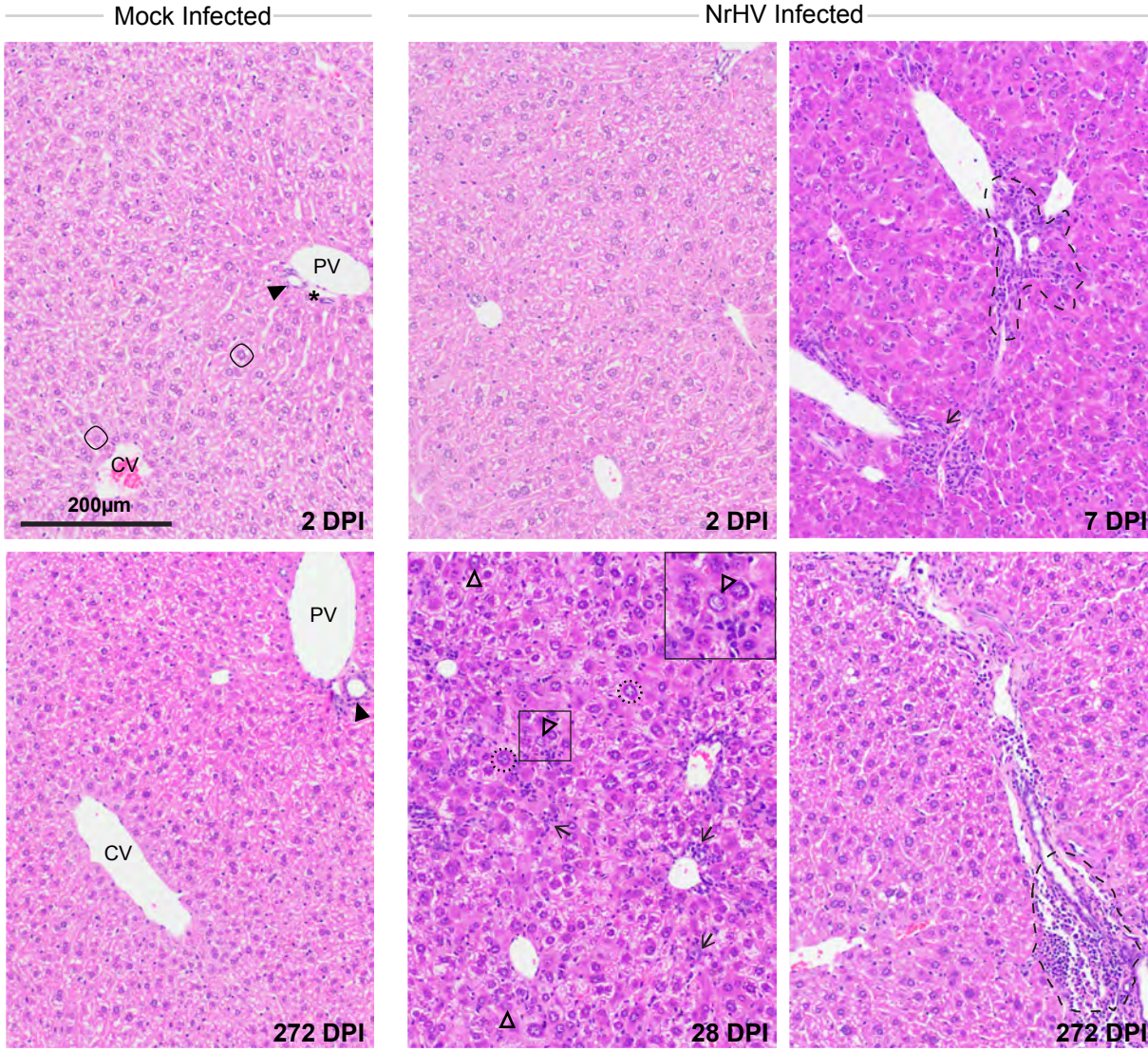

Key: PV Portal vein CV Central vein * Hepatic artery ○ Hepatocyte ▲ Bile duct ◌ Karyomegaly
↑ Hepatic necrosis △ Hepatocyte nuclear inclusions ↑ Inflammatory cells Moderate lymphocytic infiltration

Figure S13

CC080

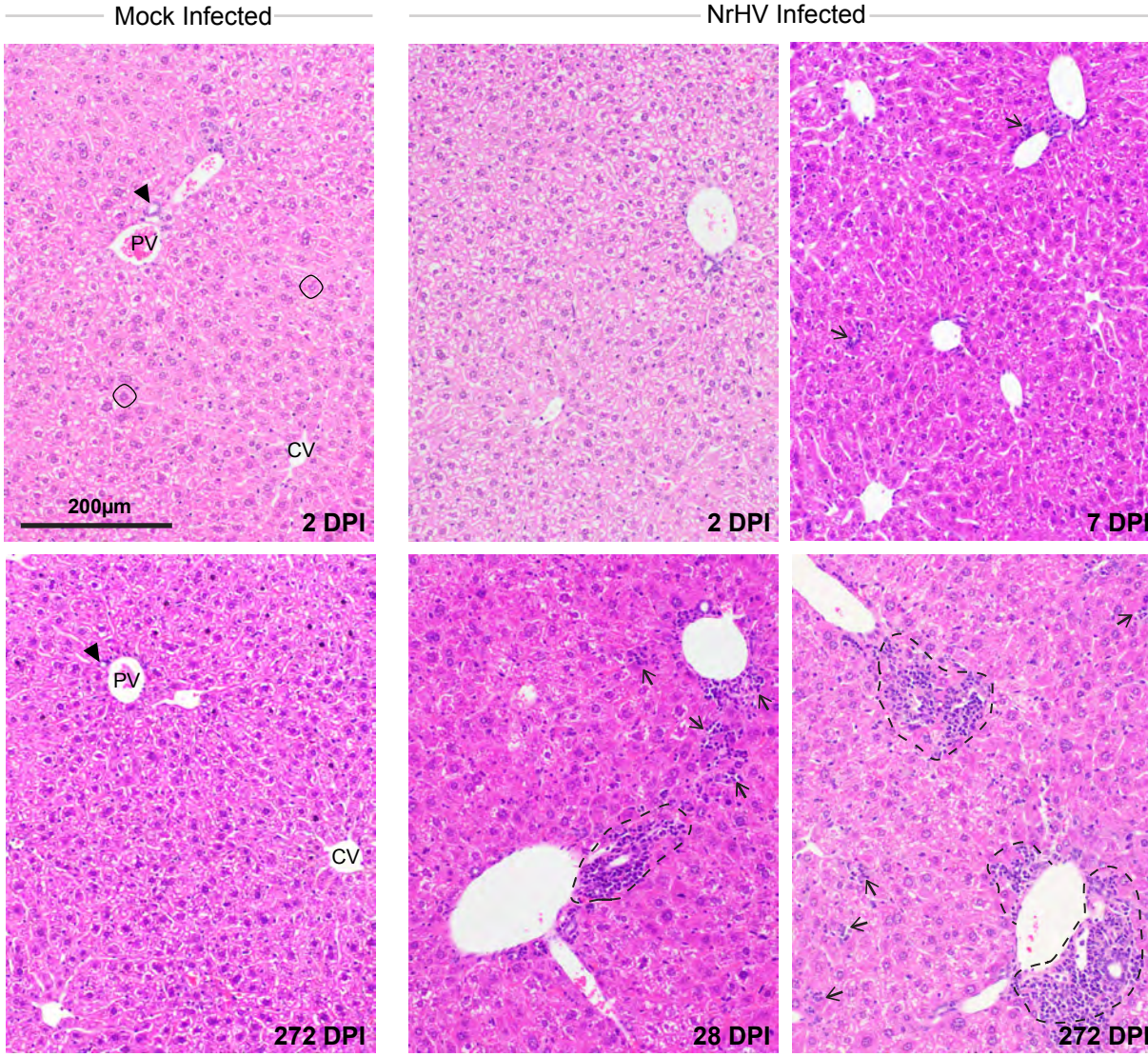

Key: PV Portal vein CV Central vein ○ Hepatocyte ▲ Bile duct
↑ Inflammatory cells Moderate lymphocytic infiltration

Figure S14

Summary of Phenotypic Data

Mouse Strain	Clearance phenotype	% Virus clearance	Infection freq. at early times	Amount Viral RNA per cell	Host response	Liver pathology	Liver Fibrosis
C57BL/6J		100% (15/15)	+	+	+++	+	-
CC046		100% (10/10)	+++	+	+	+	-
CC071		33% (5/15)	+	+++	++	+++	+++
CC080		89% (8/9)	+	+	+	++	-

Symbol/Color Key

Clearance Phenotype

- Early Clearance (< Week 3)
- Middle Clearance (Week 4-7)
- Late Clearance (Week 8-22)
- No Clearance (Week 23-EOS)

Phenotype/response level

+++ = high
++ = medium
+ = low
- = absent

Figure S15